

Semantic Forwarding and Codebook-Enhanced Model Division Multiple Access for Satellite-Terrestrial Networks

Jinghong Huang, Mengying Sun, *Member, IEEE*, Xiaodong Xu, *Senior Member, IEEE*, Jianchi Zhu, Zechuan Fang, Jingxuan Zhang, *Member, IEEE*, Ruichen Zhang, *Member, IEEE*, Chen Dong, Ping Zhang, *Fellow, IEEE*, Dusit Niyato, *Fellow, IEEE*

Abstract—Satellite-terrestrial communications are severely constrained by high path loss, limited spectrum resources, and time-varying channel conditions, rendering conventional bit-level transmission schemes inefficient and fragile, particularly in low signal-to-noise ratio (SNR) regimes. Semantic communication has emerged as a promising paradigm to address these challenges by prioritizing task-relevant information over exact bit recovery. In this paper, we propose a semantic forwarding-based semantic communication (SFSC) framework optimized for satellite-terrestrial networks. Specifically, we develop a vector-quantized joint semantic coding and modulation scheme, in which the semantic encoder and semantic codebook are jointly optimized to shape the constellation symbol distribution, improving channel adaptability and semantic compression efficiency. To mitigate noise accumulation and reduce on-board computational burden, we introduce a satellite semantic forwarding mechanism, enabling relay satellites to forward signals directly at the semantic level without full decoding and re-encoding. Furthermore, we design a channel-aware semantic reconstruction scheme based on feature-wise linear modulation (FiLM) to fuse the received SNR with semantic features, enhancing robustness under dynamic channel conditions. To support multi-user access, we further propose a codebook split-enhanced model division multiple access (CS-MDMA) method to improve spectral efficiency. Simulation results show that the proposed SFSC framework achieves a peak signal-to-noise ratio (PSNR) gain of approximately 7.9 dB over existing benchmarks in the low-SNR regime, demonstrating its effectiveness for robust and spectrum-efficient semantic transmission in satellite-terrestrial networks.

Index Terms—Satellite-terrestrial networks, semantic communication, vector quantization, semantic codebook, model division multiple access (MDMA).

This paper is supported by the National Natural Science Foundation of China No. 62401074 and No. U24B20131, and in part by the Beijing Natural Science Foundation No. L242012. (*Corresponding author: Mengying Sun*)

Jinghong Huang is with the State Key Laboratory of Networking and Switching Technology, Beijing University of Posts and Telecommunications, Beijing 100876, China, and also with the 6G Research Centre, China Telecom Beijing Research Institute, Beijing 102209, China (email: huangjh@bupt.edu.cn).

Mengying Sun, Xiaodong Xu, Zechuan Fang, Chen Dong and Ping Zhang are with the State Key Laboratory of Networking and Switching Technology, Beijing University of Posts and Telecommunications, Beijing 100876, China (email: smy_bupt@bupt.edu.cn, xuxiaodong@bupt.edu.cn, zechuan@bupt.edu.cn, dongchen@bupt.edu.cn, pzhang@bupt.edu.cn).

Jianchi Zhu is with the 6G Research Centre, China Telecom Beijing Research Institute, Beijing 102209, China (e-mail: zhujc@chinatelecom.cn).

Jingxuan Zhang is with the National School of Elite Engineering, University of Science and Technology Beijing, Beijing 100083, China (email: zhangjingxuan@ustb.edu.cn).

Ruichen Zhang and Dusit Niyato are with the College of Computing and Data Science, Nanyang Technological University, Singapore 639798 (e-mail: ruichen.zhang@ntu.edu.sg, dniyato@ntu.edu.sg)

I. INTRODUCTION

A. Background and Motivation

WITH the rapid development of various emerging applications such as artificial intelligence (AI) and the internet of everything (IoE), the forthcoming 6G networks are envisioned to establish a framework for ubiquitous intelligence and global connectivity [1]. By 2030, it is projected that over 100 billion smart devices will be connected globally, with a significant portion operating in remote, rural, or infrastructure-scarce regions [2], [3]. To accommodate these escalating demands, the vision of 6G transcends traditional terrestrial boundaries, aiming to establish a space-air-ground integrated network (SAGIN) for seamless and ubiquitous connectivity [4], [5]. In this context, non-terrestrial networks (NTN), particularly low earth orbit (LEO) satellite constellations, have emerged as indispensable parts of the 6G infrastructure [6]. LEO satellites offer distinct advantages in scalability, wide-area coverage, and deployment flexibility, making them critical for diverse applications ranging from emergency response and remote area coverage to space science data transmission.

To fully exploit the coverage potential of LEO constellations and extend connectivity to remote areas, satellite relay communication is widely recognized as a pivotal solution in the 6G network architecture [7], [8], [9]. By deploying satellite relay nodes to assist in signal transmission, this strategy effectively mitigates path blockage and extends communication range, thereby improving link robustness and system reliability [10]. Generally, depending on the on-board processing capabilities, existing satellite relay schemes can be categorized into two primary modes: transparent mode and regenerative mode [11]. Transparent mode changes the frequency carrier of the received uplink RF signal, filters and amplifies it before transmitting it on the downlink. In contrast, regenerative mode has on top of RF filtering, frequency conversion and amplification also on-board processing capabilities (for demodulation/decoding, switching and/or routing, coding/modulation), which effectively mitigates noise accumulation but incurs higher computational overhead.

Despite an immense potential of satellite relay communication, reliable transmission faces fundamental challenges inherent to varying channel conditions. Specifically, LEO satellite links are characterized by short visibility windows, highly dynamic Doppler shifts, and severe path loss [12],

[13]. These factors, combined with stringent constraints on spectrum and power budgets, make it increasingly difficult to guarantee efficient information delivery using conventional methods [14]. In such harsh environments, relying on traditional bit-level communications, which strive to faithfully recover every transmitted symbol regardless of its content, often results in excessive overhead and fragile performance [15]. To address these bottlenecks, semantic communication has emerged as a transformative paradigm [16]. By shifting the design objective from accurate bit reconstruction to the delivery of task-relevant information, semantic communication provides a pivotal solution for enhancing satellite-terrestrial networks, especially under resource-constrained conditions. Specifically, it uses shared knowledge bases, such as semantic codebooks and model priors, to extract essential semantic features while suppressing redundancy [17].

Specifically, the emerging paradigm of semantic communication primarily addresses two fundamental challenges: (i) it focuses on how to efficiently extract and compress the intrinsic semantic information from raw data to minimize redundancy while preserving the core meaning [18], [19]. (ii) it emphasizes the joint design of the transmitter and receiver to implement robust source-channel coding, which ensures semantic fidelity against the composite effects of physical channel noise and semantic noise [20], [21], [22]. When applied to the specific context of satellite networks, these two capabilities offer a tailored solution to the inherent constraints of satellite communications. On the one hand, the requirement for high-efficiency semantic extraction aligns directly with the stringent spectrum and power budgets of satellites. By transmitting only task-relevant semantic information rather than massive raw data, the system significantly alleviates the pressure on limited bandwidth resources and on-board energy consumption. In particular, the emergence of model division multiple access (MDMA) opens up a new dimension in the semantic domain, offering a novel paradigm to accommodate massive connectivity within spectrum-scarce satellite networks, thereby enhancing aggregate spectral efficiency [23]. On the other hand, the robust joint source-channel design is indispensable for overcoming harsh channel conditions typical of LEO links. Facing severe path loss and dynamic Doppler shifts caused by high-mobility nodes, semantic-based transmission provides a resilient mechanism to recover information even in low signal-to-noise ratio (SNR) regimes.

Nevertheless, the deployment of semantic communication in LEO satellite relay networks is still in its infancy and faces unique challenges that cannot be directly addressed by existing terrestrial frameworks [24]. First, most current research focuses on point-to-point links, neglecting the semantic noise accumulation inherent in satellite relay systems [25]. In a satellite dual-hop or multi-hop architecture, the semantic distortion introduced in the uplink may be amplified during downlink transmission, leading to severe degradation of the end-to-end semantic fidelity. Second, existing MDMA paradigms are constrained by their reliance on either inter-user common information or strict model orthogonality, thereby severely limiting the achievable spectral efficiency for inde-

pendent user tasks. Third, the semantic communication models are computationally intensive. Deploying complex encoders or decoders directly on energy-constrained satellite payloads requires a delicate trade-off between semantic performance and on-board computational overhead, which remains an open issue. Furthermore, LEO channels exhibit rapid time-varying characteristics. Semantic communication models, trained on static channel models, face a critical generalization challenge due to the significant discrepancy between the static training assumptions and the complex, fluctuating propagation conditions of satellite networks. Consequently, these unresolved issues motivate the need for a resilient, efficient, and channel-adaptive semantic relay framework tailored for 6G satellite-terrestrial networks, which constitutes the primary focus of this paper.

B. Related Work

This subsection reviews the existing research regarding the convergence of semantic communication and satellite networks. We begin by exploring the integration of semantic paradigms into satellite networks, tracing the evolution from terrestrial point-to-point links to cooperative satellite relay scenarios. Furthermore, we extend our review to the multiple access domain by investigating the recent advances in MDMA and analyzing their limitations in resource-constrained satellite environments.

1) *Semantic Communication for Satellite Networks:* Early semantic communication frameworks were predominantly designed for terrestrial scenarios, initially relying on analog transmission [15]. To bridge the gap with modern digital standards, recent efforts have pivoted towards digital implementations. For instance, to resolve the non-differentiability issue of digital modulation, Tung et al. [26] incorporated constellation constraints into the end-to-end training process, thereby maintaining performance close to unconstrained schemes. Fu et al. [27] proposed a deep learning-enabled vector quantized semantic communication framework, which leverages discrete codebooks to significantly enhance feature robustness over digital channels. Furthermore, the probabilistic mapping from source data to discrete constellations was modeled via a variational autoencoder (VAE) by Bo et al. [28], effectively optimizing the mapping between semantic features and channel symbols. While these studies successfully adapt semantic transmission to digital hardware, they primarily assume static or slowly varying channel conditions. Consequently, they lack specific mechanisms required to combat the extreme Doppler shifts and rapid phase variations inherent in high-mobility satellite links.

Recognizing the unique challenges of satellite networks, recent research has extended semantic paradigms to satellite networks. To mitigate the Doppler effect and channel noise, semantic coding has been integrated with orthogonal time-frequency space (OTFS) modulation [29] and robust joint coding-modulation mechanisms [30]. regarding resource efficiency, on-board semantic filtering [31] and generative AI-based reconstruction [32] were proposed to minimize transmission overhead. However, these works predominantly focus

on single-hop links. While [32] considers a relay scenario, it treats the satellite as a conventional regenerative node performing bit-level orthogonal frequency division multiplexing (OFDM) demodulation and remodulation. Such approaches render the satellite agnostic to the semantic information, thereby failing to address the semantic noise accumulation inside the relay node or exploit the potential of on-board semantic processing for further efficiency.

To alleviate severe propagation loss in satellite networks, semantic relay serves as an effective approach to enhance link reliability by performing feature-level regeneration. Ma et al. [33] validated this approach, showing that intelligent semantic relay significantly outperforms simple amplification forward in varying channel conditions. To resolve the issue of mismatched knowledge bases, Luo et al. [34] proposed the semantic forwarding (SF), which enables relay nodes to act as semantic translators, bridging the knowledge discrepancy between the source and the destination without shared knowledge base. Complementing these studies, An et al. [35] addressed visual tasks by implementing secondary compression at the relay, effectively reducing forwarding overhead. However, these frameworks are largely confined to static terrestrial environments and standard channel models. They fail to address the unique challenges of LEO satellite networks, such as rapid Doppler shifts and severe propagation delays, which create rigorous generalization barriers. Moreover, the high computational cost of current semantic re-encoding modules is often incompatible with the stringent power constraints of satellite payloads, highlighting the urgent need for lightweight, channel-adaptive solutions.

2) Multiple Access Techniques for Satellite Networks:

To achieve massive connectivity within limited spectrum resources, particularly in satellite networks, extensive research has been conducted on various novel multiple access techniques, such as rate-splitting multiple access (RSMA) and non-orthogonal multiple access (NOMA) [36], [37]. The concept of MDMA was formally introduced in [23], thereby opening up a new dimension in the semantic domain to further enhance spectral efficiency. By mining and reusing the shared semantic information of multiple users in the model information space, this scheme significantly saves transmission bandwidth and achieves performance superior to traditional NOMA techniques in the low SNR regime. On this basis, Liang et al. [38] further proposed an orthogonal MDMA (O-MDMA). Leveraging the semantic orthogonality among different models, this method transforms the capability of deep joint source-channel coding (DeepJSCC) model from combating channel noise to suppressing multi-user interference. However, the semantic orthogonality between different models remains difficult to guarantee. Therefore, Wu et al. [39] proposed a joint deep adversarial semantic decomposition (JDASD) scheme to address the multi-user interference issue in MDMA systems, utilizing a generative adversarial network (GAN) to enforce mutually exclusive mappings in the model space. Furthermore, Ma et al. [40] utilized the robust information bottleneck (RIB) theory to effectively reduce multi-user interference and protect user privacy in inference and reconstruction tasks. However, frameworks designed for terrestrial

networks are inadequate for LEO satellite networks. They neglect semantic noise accumulation in multi-hop scenarios, impose computational burdens exceeding satellite power constraints, and rely on static channel models. Consequently, developing a lightweight and robust semantic relay framework remains a critical necessity.

C. Contributions and Paper Structure

This paper aims to develop a semantic forwarding-based semantic communication (SFSC) framework for satellite networks. By integrating efficient semantic compression, lightweight relay operations, robust semantic recovery, and scalable multi-user support, we seek to establish a lightweight, end-to-end trainable satellite communication architecture. The primary contributions are as follows.

- We propose a satellite semantic forwarding mechanism that enables satellite relay nodes to forward received signals at the semantic level. This mechanism mitigates channel noise accumulation and improves robustness against channel impairments. Furthermore, this direct semantic forwarding strategy operates without full decoding and re-encoding, which prevents semantic noise accumulation and significantly reduces on-board computational overhead.
- We develop a vector-quantized joint coding and modulation framework in which a learnable semantic codebook performs joint semantic compression and constellation mapping, enabling efficient end-to-end transmission of semantic features.
- We design a channel-aware semantic reconstruction scheme by injecting SNR information into the recovery modules, thereby enhancing adaptivity and stability under time-varying satellite channels.
- We extend the proposed system to multi-user scenarios and propose a semantic codebook split-enhanced MDMA (CS-MDMA) approach, achieving higher throughput and spectral efficiency while sharing model parameters across users.
- Simulation results under realistic LEO channel models show that the proposed framework significantly outperforms existing benchmarks, achieving a peak signal-to-noise ratio (PSNR) gain of approximately 7.9 dB in the low SNR regime while reducing the on-board model parameters by 84% compared to conventional regenerative joint coding-modulation schemes.

Overall, the SFSC framework provides a viable and efficient architecture for deploying semantic communication in satellite networks. Extensive experiments demonstrate the system's superior performance in terms of semantic reconstruction quality, channel adaptability and multi-user support.

The rest of the paper is organized as follows. In Section II, we present the satellite channel model and introduce our proposed SFSC framework for satellite networks in detail. Section III further introduces our proposed codebook split-enhanced model division multiple access approach. In Section IV, we evaluate the performance of our proposed framework through extensive experiments. Finally, Section V

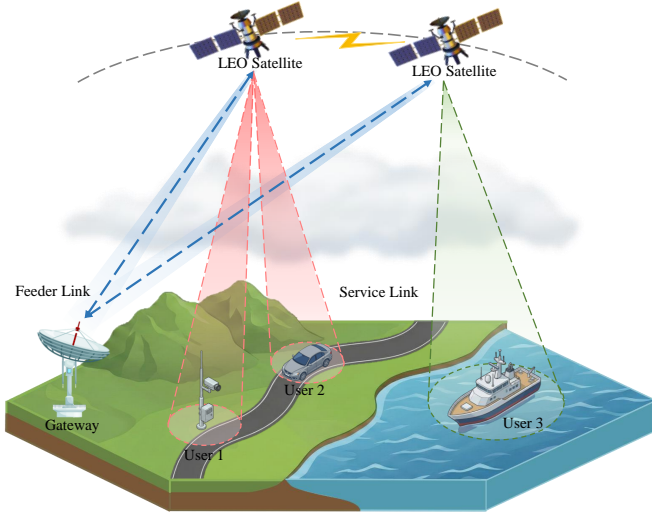


Fig. 1: System model of relay-assisted LEO satellite-terrestrial communications. The ground gateway connects to the satellite via the feeder link, while the satellite serves multiple users through the service link. Furthermore, different satellites are interconnected via inter-satellite links to achieve wider network coverage.

concludes the paper. The main notations are summarized in Table I.

II. SFSC FRAMEWORK FOR SATELLITE-TERRESTRIAL NETWORKS

In this section, we investigate an application of semantic forwarding within satellite relay scenarios, with a specific focus on the transmitter and receiver designs for terrestrial user terminals (UT) and gateways, as well as the semantic forwarder for satellite nodes. We first formulate the LEO satellite channel and signal models, and establish an overall architecture for semantic forwarding-based semantic communication system for satellite networks. Building on this, we propose a channel-adaptive semantic forwarding and reconstruction scheme with SNR awareness, thereby ensuring robust performance across a broader range of channel conditions. Finally, we formulate the specific loss function designs and elaborate on the joint training methodology of the proposed models.

A. Channel and Signal Model

1) *Channel Model*: As shown in Fig. 1, we consider a relay-assisted satellite-terrestrial communication system with a single antenna LEO satellite, where the satellite can provide services to multiple user terminals at the same time.

Taking the feeder downlink channel between the satellite and the gateway as an example, a short time slot is considered, where the relative positions of the satellite and the gateway do not change significantly during a time slot, and the scattering environment is assumed to be smooth in the target interval under consideration. The complex baseband feeder downlink space domain channel response between the satellite and the gateway at moment t and frequency f can be expressed as follows [41], [42]:

$$h^{dl}(t, f) = \exp\{\bar{j}2\pi [t\nu^{sat} - f\tau]\} \cdot g^{dl}(t, f), \quad (1)$$

where ν^{sat} is the Doppler shift caused by the motion of the LEO satellite, τ is the propagation delay, $\bar{j} = \sqrt{-1}$, and $g^{dl}(t, f)$ represents the feeder downlink channel gain. The statistical properties of the channel gain $g^{dl}(t, f)$ in LEO satellite communications mainly depend on the propagation environment in which the UT is located. We primarily consider the case where both line-of-sight (LoS) and non-line-of-sight (NLoS) propagation exist simultaneously. Therefore, the feeder downlink channel gain $g^{dl}(t, f)$ exhibits the Rician distribution with the Rician factor k and power γ_r [43].

Similarly, the complex baseband service uplink space domain channel response between the UT and the satellite at moment t and frequency f can be expressed as

$$h^{ul}(t, f) = \exp\{\bar{j}2\pi [t\nu^{sat} - f\tau]\} \cdot g^{ul}(t, f), \quad (2)$$

where ν^{sat} is the Doppler shift caused by the motion of the LEO satellite, τ is the propagation delay, and $g^{ul}(t, f)$ represents the service uplink channel gain.

2) *Signal Model*: Taking the feeder downlink channel between the satellite and the gateway as an example, the received signal at the gateway is expressed as

$$y^{dl}(t) = \int_{-\infty}^{\infty} h^{dl}(t, \tau) \cdot x^{dl}(t - \tau) d\tau + z(t), \quad (3)$$

where $x^{dl}(t)$ represents the signal transmitted by the satellite, $z(t)$ denotes the additive white Gaussian noise (AWGN), $h^{dl}(t, \tau)$ is the inverse Fourier transform of $h^{dl}(t, f)$ in terms of τ .

Similarly, for the service uplink channel between the UT and the satellite, the received signal at the satellite is expressed as

$$y^{ul}(t) = \int_{-\infty}^{\infty} h^{ul}(t, \tau) \cdot x^{ul}(t - \tau) d\tau + z(t), \quad (4)$$

where $x^{ul}(t)$ represents the signal transmitted by the UT, $z(t)$ denotes the additive white Gaussian noise, $h^{ul}(t, \tau)$ is the inverse Fourier transform of $h^{ul}(t, f)$ in terms of τ .

B. System Model of SFSC

1) *Model Design of Terrestrial User Terminal*: As shown in Fig. 2, the UT input image is denoted as \mathbf{X} . The original image is mapped from the original color space to the semantic space by a semantic encoder, and the semantic encoded information is denoted as

$$\mathbf{L} = f_{se}(\mathbf{X}; \theta_{se}), \quad (5)$$

where $f_{se}(\cdot; \theta_{se})$ denotes the semantic encoder with learnable parameters θ_{se} , $\mathbf{L} = [\mathbf{l}_1, \mathbf{l}_2, \dots, \mathbf{l}_M]^T \in \mathbb{R}^{M \times N}$, M represents the number of feature vectors, and N represents the dimension of each vector. The semantic encoded information is quantized according to the distance between the semantic feature vectors and the codebook vectors, and the original semantic feature vectors are replaced using the indices of the codebook vectors. The trained codebook is represented as $\mathbf{E} = [\mathbf{e}_1, \mathbf{e}_2, \dots, \mathbf{e}_K]^T \in \mathbb{R}^{K \times N}$, with K representing the number of codebook vectors. The vector quantization process is expressed as [44]

$$k^{index} = \text{VQ}(\mathbf{L}; \mathbf{E}), \quad (6)$$

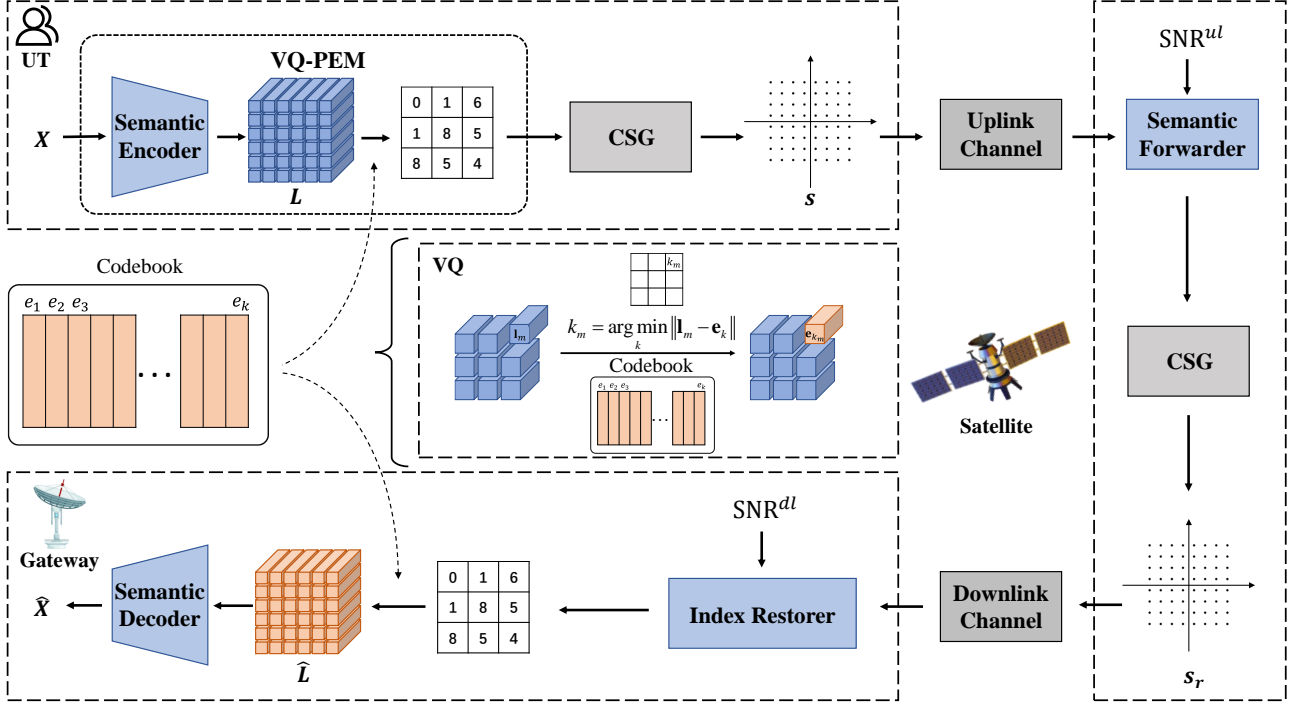


Fig. 2: Semantic forwarding-based semantic communication framework for satellite-terrestrial networks. The UT encodes original image into semantic codebook indices via VQ-PEM. The satellite utilizes a semantic forwarder to encode the received signal into recovered semantic codebook indices. The gateway reconstructs image via index restoration and semantic decoding.

where $k^{index} = [k_1, k_2, \dots, k_M] \in \mathbb{R}^M$, $k_m = \underset{k}{\operatorname{argmin}} \|l_m - e_k\|$, $m \in \{1, \dots, M\}$, $k \in \{1, \dots, K\}$.

In order to achieve joint semantic information encoding and modulation based on vector quantization, we combine the above semantic encoding and vector quantization processes into a vector quantized probabilistic encoder-modulator (VQ-PEM) [28] [44], where the VQ-PEM output is represented as

$$\mathbf{I} = \text{PEM}_{vq}(\mathbf{X}; \mathbf{E}; \theta_{se}), \quad (7)$$

where $\mathbf{I} = [i_1, i_2, \dots, i_M] \in \mathbb{R}^{M \times K}$, and i_m denotes the one-hot vector with the k_m -th element being 1. The quantized information \mathbf{I} is passed through a constellation symbol generator (CSG) to generate the transmission complex signal s as channel input. At the same time, due to the non-differentiability of the $\operatorname{argmin}(\cdot)$ operation, we use the ReinMax method to generate the differentiable constellation symbols [45].

Conventional gradient estimators for discrete latent variables, such as straight-through (ST) [46] and ST gumbel-softmax (STGS) [47], typically provide first-order gradient approximations. In contrast, ReinMax offers a second-order approximation leveraging the Heun method [45]. This approach significantly enhances gradient estimation accuracy without incurring the computational overhead of higher-order derivatives.

2) *Model Design of Satellite Relay Node:* The semantic forwarder at the satellite relay node learns the transfer

TABLE I: LIST OF SYSTEM MODEL NOTATIONS

Notation	Description
\mathbf{X}	Original image
$\mathbf{L} \in \mathbb{R}^{M \times N}$	The semantic encoded information
$\mathbf{E} \in \mathbb{R}^{K \times N}$	Semantic codebook
$\mathbf{I} \in \mathbb{R}^{M \times K}$	One-hot matrix of semantic codebook indices
$\bar{\mathbf{I}} \in \mathbb{R}^{M \times K}$	Recovered codebook indices at satellite
$\hat{\mathbf{I}} \in \mathbb{R}^{M \times K}$	Recovered codebook indices at gateway
$\hat{\mathbf{L}} \in \mathbb{R}^{M \times N}$	Recovered semantic feature
$\hat{\mathbf{X}}$	Recovered image
$\mathbf{E}_c \in \mathbb{R}^{K \times (P_1 + P_2)}$	Common orthogonal codebook
θ	The set of all trainable parameters
γ	FiLM scaling factor
β	FiLM shifting factor
λ_{trans}	Transmission loss weight
λ_{quant}	Quantization loss weight
\mathcal{L}	Composite loss function

probability of the transmit constellation symbols according to the fading and noise conditions of the service uplink channel and the transmit signal distribution, and recodes the received digital semantic signals. At the same time, the computational overhead of satellite regenerative forwarding is greatly reduced because complete semantic decoding and

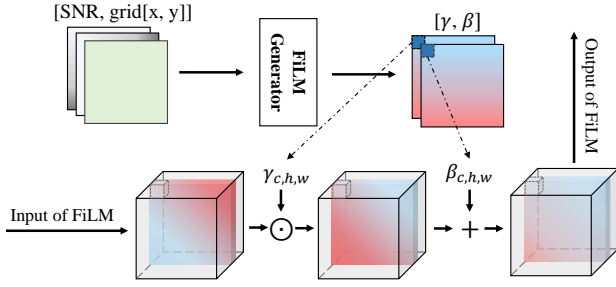


Fig. 3: Illustration of the SNR adaptive feature-wise linear modulation. By concatenating SNR with spatial coordinate maps, the generator outputs the channel scaling factor γ and channel shifting factor β to modulate intermediate feature maps via affine transformation.

recoding of the semantic information is not required. The semantic forwarding process is represented as

$$\bar{\mathbf{I}} = f_{sf}(\bar{\mathbf{s}}; \theta_{sf}), \quad (8)$$

where $f_{sf}(\cdot; \theta_{sf})$ denotes the semantic forwarder with learnable parameters θ_{sf} , $\bar{\mathbf{I}} = [\hat{\mathbf{i}}_1, \hat{\mathbf{i}}_2, \dots, \hat{\mathbf{i}}_M]^T \in \mathbb{R}^{M \times K}$. Same as the transmitter, the transmission complex signal s_r is generated as channel input by CSG.

3) *Model Design of Gateway*: As shown in Fig. 2, the gateway receiver comprises two main components, an index restorer and a semantic decoder. Similar to the semantic forwarder, the index restorer is designed to recover the original one-hot encoded indices. It achieves this by learning the posterior probabilities of the constellation symbols according to the channel fading, noise and the transmit signal distribution. The recovered one-hot indices are denoted as

$$\hat{\mathbf{I}} = f_{ir}(\hat{\mathbf{s}}_r; \theta_{ir}), \quad (9)$$

where $f_{ir}(\cdot; \theta_{ir})$ denotes the index restorer with learnable parameters θ_{ir} , $\hat{\mathbf{I}} = [\hat{\mathbf{i}}_1, \hat{\mathbf{i}}_2, \dots, \hat{\mathbf{i}}_M]^T \in \mathbb{R}^{M \times K}$.

Based on the recovered one-hot indices, combined with the semantic codebook shared by the receiver and transmitter, the recovered quantized semantic feature $\hat{\mathbf{L}}$ can be obtained. Subsequently, $\hat{\mathbf{L}}$ is processed by the semantic decoder to obtain the reconstructed image, denoted as

$$\hat{\mathbf{X}} = f_{sd}(\hat{\mathbf{L}}; \theta_{sd}), \quad (10)$$

where $f_{sd}(\cdot; \theta_{sd})$ denotes the semantic decoder with learnable parameters θ_{sd} .

C. Channel Adaptive Semantic Recovery

At the satellite relay nodes, due to the high-speed relative movement of the satellite and the ground terminals, as well as the dynamic topological conditions of the satellite constellations, the communication system often needs to ensure the reliability of operation over wide SNR range. Different channel SNR conditions will have a significant impact on the received signals, thus affecting the receiver's error correction or recovery performance. In order to improve the robustness of the proposed system to dynamic channel conditions, we combine the SNR with the received signals as input to the

relay semantic forwarder, denoted as $\bar{\mathbf{s}}_{snr} = [\boldsymbol{\mu}_1, \bar{\mathbf{s}}]$, where $\boldsymbol{\mu}_1$ denotes the sequence with the same shape as $\bar{\mathbf{s}}$, and the value is the current SNR value. The above equation (8) is rewritten as

$$\bar{\mathbf{I}} = f_{sf}(\bar{\mathbf{s}}_{snr}; \theta_{sf}). \quad (11)$$

Similarly, at the gateway, the received signal $\hat{\mathbf{s}}_r$ is combined with the feeder downlink SNR $\boldsymbol{\mu}_2$ to $\hat{\mathbf{s}}_{snr} = [\boldsymbol{\mu}_2, \hat{\mathbf{s}}_r]$, and the above equation (9) is rewritten as

$$\hat{\mathbf{I}} = f_{ir}(\hat{\mathbf{s}}_{snr}; \theta_{ir}). \quad (12)$$

Note that although CSI feedback and interference prediction have been extensively studied, obtaining accurate CSI at the transmitter remains a challenge due to the large propagation delays and the mobility of both satellites and user terminals. At the receiver, CSI can be reliably estimated utilizing pilot signals or other reference information. Therefore, we believe that it is reasonable and necessary to incorporate SNR into the semantic forwarder at the satellite relay node and the index restorer at the gateway.

As illustrated in Fig. 3, to enable effective guidance of model inference by the SNR, we further propose a semantic feature fusion method based on spatially adaptive feature-wise linear modulation (FiLM) [48]. Departing from conventional global modulation, and to address the spatially non-uniform characteristics of feature representations, we leverage coordinate convolution [49]. Specifically, by concatenating normalized spatial coordinate maps $grid[x, y]$ to the input of the FiLM generator, the generator is able to perceive the absolute spatial locations within the feature map.

On this basis, two channel-related factors are introduced, the channel scaling factor γ and the channel shifting factor β . The FiLM generator with learnable parameters θ_g outputs γ and β based on the current SNR. Taking the service uplink as an example, the FiLM factors are expressed as

$$\gamma, \beta = f_g(\boldsymbol{\mu}_1, \theta_g). \quad (13)$$

Specifically, the intermediate feature maps undergo an affine transformation, defined by the generated scale and shift parameters. This mechanism enables dynamic adaptation of the information reconstruction process in response to channel variations. The mathematical expression is given by

$$\text{FiLM}(\mathbf{F}_{c,h,w}^{mid}, \gamma_{c,h,w}, \beta_{c,h,w}) = \gamma_{c,h,w} \cdot \mathbf{F}_{c,h,w}^{mid} + \beta_{c,h,w}, \quad (14)$$

where $\mathbf{F}_{c,h,w}^{mid}$ denotes the activation value of the c -th feature map at spatial coordinate $[h, w]$ in the intermediate layer of the model, and $\gamma_{c,h,w}$ and $\beta_{c,h,w}$ are the corresponding scaling and shifting parameters generated at the same spatial location, respectively. Through this mechanism, the model achieves fine-grained feature restoration across different channel conditions and spatial regions.

D. Training Process

To develop an end-to-end image semantic communication system that achieves both high fidelity and robustness over satellite relay channels, it is essential to jointly optimize three inherently coupled objectives: UT-side reconstruction

Algorithm 1: SFSC Training Algorithm

Initialization: Initialize the model parameters θ , training dataset \mathcal{D} , epoch number E and batch size B .

for $t = 1$ **to** E **do**

Select mini-batch data $\{\mathbf{X}\}_{i=n}^{n+B}$ from \mathcal{D}
 Semantic encoding: $\{\mathbf{X}\}_{i=n}^{n+B} \xrightarrow{f_{se}(\cdot; \theta)} \{\mathbf{L}\}_{i=n}^{n+B}$
 Vector quantization and CSG:
 $\{\mathbf{L}\}_{i=n}^{n+B} \xrightarrow{VQ, CSG} \{\mathbf{s}\}_{i=n}^{n+B}$
 Satellite uplink channel: $\{\mathbf{s}\}_{i=n}^{n+B} \longrightarrow \{\hat{\mathbf{s}}\}_{i=n}^{n+B}$
 Satellite forwarding:
 $\{\hat{\mathbf{s}}\}_{i=n}^{n+B} \xrightarrow{f_{sf}(\cdot; \theta)} \{\hat{\mathbf{I}}\}_{i=n}^{n+B} \xrightarrow{CSG} \{\mathbf{s}_r\}_{i=n}^{n+B}$,
 Satellite downlink channel: $\{\mathbf{s}_r\}_{i=n}^{n+B} \longrightarrow \{\hat{\mathbf{s}}_r\}_{i=n}^{n+B}$
 Index recovery:
 $\{\hat{\mathbf{s}}_r\}_{i=n}^{n+B} \xrightarrow{f_{ir}(\cdot; \theta)} \{\hat{\mathbf{I}}\}_{i=n}^{n+B}$
 Vector de-quantization and semantic decoding:
 $\{\hat{\mathbf{I}}\}_{i=n}^{n+B} \xrightarrow{VDQ} \{\hat{\mathbf{L}}\}_{i=n}^{n+B} \xrightarrow{f_{sd}(\cdot; \theta)} \{\hat{\mathbf{X}}\}_{i=n}^{n+B}$
 Compute loss $\mathcal{L}(\theta)$
 Update θ through gradient descent with $\mathcal{L}(\theta)$

return Trained parameters θ

quality, transmission reliability over the relay channel, and quantization distortion. To this end, we formulate the training procedure of the entire system as a multi-objective optimization problem. Let $\theta = \{\theta_{se}, \theta_{sf}, \theta_{ir}, \theta_{sd}, \mathbf{E}\}$ denote the set of all trainable parameters, encompassing every network weight from the transmitter-side semantic encoder to the receiver-side semantic decoder. Our goal is to obtain the optimal parameter set θ^* that minimizes the composite loss function $\mathcal{L}(\theta)$, which can be expressed as

$$\theta^* = \arg \min_{\theta} \mathcal{L}(\theta), \quad (15)$$

where $\mathcal{L}(\theta) = \mathcal{L}_{rec}(\theta) + \lambda_{trans} \mathcal{L}_{trans}(\theta) + \lambda_{quant} \mathcal{L}_{quant}(\theta)$. The composite loss consists of three components, the end-to-end reconstruction loss \mathcal{L}_{rec} , the reliable transmission loss \mathcal{L}_{trans} , and the quantization regularization loss \mathcal{L}_{quant} . The hyperparameters λ_{trans} and λ_{quant} control the relative importance of these terms within the overall optimization process. The following sections provide a detailed explanation of each loss component.

The primary objective of the proposed system is to minimize the distortion between the original source image \mathbf{X} and the reconstructed image $\hat{\mathbf{X}}$ at the receiver, thereby ensuring fidelity at the task level. From an information-theoretic perspective, minimizing distortion aligns with maximizing the amount of source information preserved in the received features. Accordingly, following the Info-Max principle [50], the core theoretical objective of the system is formulated as maximizing the mutual information between the downlink channel output features $\hat{\mathbf{s}}_r$ and the original source \mathbf{X} , denoted by $I_{\theta}(\mathbf{X}; \hat{\mathbf{s}}_r)$.

Since directly computing mutual information in high-dimensional spaces is computationally intractable, we adopt variational inference to indirectly optimize the system param-

eters by maximizing the Barber-Agakov lower bound of the mutual information [51],

$$I_{\theta}(\mathbf{X}; \hat{\mathbf{s}}_r) \geq H(\mathbf{X}) + \mathbb{E}_{p(\mathbf{X}, \hat{\mathbf{s}}_r)}[\log q(\mathbf{X} | \hat{\mathbf{s}}_r)]. \quad (16)$$

For the reconstruction task, this objective specifically reduces to maximizing the expected log-likelihood of the original data under the decoder,

$$\mathcal{J}_{rec} = \mathbb{E}_{p(\mathbf{X}, \hat{\mathbf{s}}_r)}[\log q(\mathbf{X} | \hat{\mathbf{s}}_r)], \quad (17)$$

where the expectation \mathbb{E} is taken with respect to the true joint distribution $p(\mathbf{X}, \hat{\mathbf{s}}_r)$, and $q(\mathbf{X} | \hat{\mathbf{s}}_r)$ denotes the approximate posterior distribution parameterized by the decoder.

To make the log-likelihood objective tractable, we introduce a Gaussian assumption. Specifically, the posterior distribution of the original image source \mathbf{X} conditioned on the received signal $\hat{\mathbf{s}}_r$ is modeled as a multivariate isotropic Gaussian distribution, given by

$$q(\mathbf{X} | \hat{\mathbf{s}}_r) = \mathcal{N}(\boldsymbol{\mu}, \sigma^2 \mathbf{I}_{k \times k}). \quad (18)$$

The mean parameter $\boldsymbol{\mu}$ is parameterized by the decoder output, i.e., $\boldsymbol{\mu} = f_{de}(\hat{\mathbf{s}}_r)$, while the variance σ^2 is fixed, and k denotes the dimensionality of the original image source. Substituting this probability density function into the objective \mathcal{J}_{rec} , expanding it using the properties of the logarithm, and applying the linearity of the expectation operator, we obtain

$$\begin{aligned} \mathcal{J}_{rec} &= \mathbb{E}_{p(\mathbf{X}, \hat{\mathbf{s}}_r)} \left[\log \left(\frac{1}{(2\pi)^{k/2} \sigma} \exp \left(-\frac{\|\mathbf{X} - f_{de}(\hat{\mathbf{s}}_r)\|_2^2}{2\sigma^2} \right) \right) \right] \\ &= \mathbb{E}_{p(\mathbf{X}, \hat{\mathbf{s}}_r)} \left[-\frac{1}{2\sigma^2} \|\mathbf{X} - f_{de}(\hat{\mathbf{s}}_r)\|_2^2 + C \right] \\ &= -\frac{1}{2\sigma^2} \mathbb{E}_{p(\mathbf{X}, \hat{\mathbf{s}}_r)} [\|\mathbf{X} - f_{de}(\hat{\mathbf{s}}_r)\|_2^2] + C, \end{aligned} \quad (19)$$

where $f_{de}(\cdot)$ denotes the actual decoding process that recovers the reconstructed image from the received signal, and C denotes a constant independent of the optimization variables. Accordingly, the final end-to-end reconstruction loss \mathcal{L}_{rec} is defined as

$$\mathcal{L}_{rec}(\theta) = \mathbb{E}_{p(\mathbf{X}, \hat{\mathbf{s}}_r)} [\|\mathbf{X} - f_{de}(\hat{\mathbf{s}}_r)\|_2^2]. \quad (20)$$

Although the end-to-end reconstruction loss \mathcal{L}_{rec} can supervise the recovery of global semantic information, when signals propagate through a high-noise dual-hop satellite relay channel, the gradients used to optimize the transmitter and relay parameters may suffer from vanishing gradient, making the model difficult to converge [52] [53]. To mitigate this issue and impart explicit denoising capabilities to the relay and receiver, it is necessary to introduce a reliable transmission loss \mathcal{L}_{trans} .

The objective of the relay node and receiver is to accurately recover the discrete semantic features transmitted from the source. According to the Info-Max principle, ensuring reliable transmission over the S-R-D link is equivalent to maximizing the mutual information between the discrete indices $\mathbf{I} \in \{0, 1\}^{M \times K}$ and the received signal at the gateway $\hat{\mathbf{s}}$, namely $I_{\phi}(\mathbf{I}; \hat{\mathbf{s}})$, where the parameter set $\phi \subset \theta$.

Similar to the reconstruction task, since mutual information is generally intractable to compute directly, we again adopt

$$\begin{aligned} \mathcal{L}(\boldsymbol{\theta}) = & \frac{1}{N_b} \sum_{i=1}^{N_b} \left(\|\mathbf{X}^{(i)} - f_{de}(\hat{\mathbf{s}}_r^{(i)})\|_2^2 - \lambda_{trans} \sum_{m=1}^M \sum_{k=1}^K \mathbf{I}_{m,k}^{(i)} \log \left(q_\phi(\mathbf{I}_m^{(i)} = k \mid \hat{\mathbf{s}}^{(i)}) \right) \right. \\ & \left. + \lambda_{quant} \left(\|\text{sg}[\mathbf{L}^{(i)}] - \mathbf{L}_{vq}^{(i)}\|_2^2 + \beta_q \|\mathbf{L}^{(i)} - \text{sg}[\mathbf{L}_{vq}^{(i)}]\|_2^2 \right) \right) \end{aligned} \quad (21)$$

a variational inference framework. Specifically, a variational posterior distribution $q_\phi(\mathbf{I} \mid \hat{\mathbf{s}})$ is introduced to approximate the true posterior, where $q_\phi(\cdot)$ is parameterized by the index restorer at the gateway. The system parameters are optimized by maximizing the expected log-likelihood term $\mathbb{E}[\log q_\phi(\mathbf{I} \mid \hat{\mathbf{s}})]$.

For the discrete semantic index \mathbf{I} , which belongs to a finite constellation set (e.g., 64-QAM), the Gaussian assumption is no longer appropriate. Therefore, the variational posterior distribution $q_\phi(\mathbf{I} \mid \hat{\mathbf{s}})$ is modeled as a multinomial distribution.

To address the computational complexity associated with high-dimensional joint distributions, we adopt the mean field approximation from variational inference. Under this assumption, conditioned on the received signal $\hat{\mathbf{s}}$, the semantic symbols in the sequence are assumed to be conditionally independent [54]. As a result, the joint variational posterior distribution is factorized as

$$q_\phi(\mathbf{I} \mid \hat{\mathbf{s}}) = \prod_{m=1}^M \prod_{k=1}^K (q_\phi(\mathbf{I}_m = k \mid \hat{\mathbf{s}}))^{\mathbf{I}_{m,k}}, \quad (22)$$

where $q_\phi(\mathbf{I}_m = k \mid \hat{\mathbf{s}})$ denotes the predicted probability that the m -th semantic symbol belongs to the k -th constellation point given the received signal $\hat{\mathbf{s}}$. This distribution is determined by the index restorer parameterized by ϕ . The exponent $\mathbf{I}_{m,k}$ is a one-hot indicator variable, which is equal to 1 if and only if the true symbol category is k , and 0 otherwise.

Substituting the above probability mass function into the log-likelihood objective and exploiting the logarithmic property that converts products into summations, we observe that maximizing the expected log-likelihood is mathematically equivalent to minimizing the cross-entropy between the predicted distribution and the truth one-hot distribution. Accordingly, the reliable transmission loss \mathcal{L}_{trans} is formulated as

$$\mathcal{L}_{trans}(\boldsymbol{\theta}) = -\mathbb{E}_{p(\mathbf{I}, \hat{\mathbf{s}})} \left[\sum_{m=1}^M \sum_{k=1}^K \mathbf{I}_{m,k} \log (q_\phi(\mathbf{I}_m = k \mid \hat{\mathbf{s}})) \right]. \quad (23)$$

Through this reliable transmission loss, the satellite relay and gateway explicitly learn the transition characteristics of the dual-hop channel while implicitly capturing the prior distribution of the original semantic indices. Consequently, the network is capable of mapping the noisy received signals back to the optimal discrete constellation points, effectively approximating the maximum a posteriori (MAP) criterion. This intermediate supervision mechanism not only alleviates the vanishing gradient problem across the dual-hop link but also endows the index restorer with error-correction capabilities by incorporating source statistics, thereby significantly enhancing end-to-end robustness under adverse channel conditions.

While the ReinMax estimator effectively circumvents the non-differentiability of the quantization operation, thereby facilitating end-to-end backpropagation, it introduces a new optimization challenge, the updates of the encoder and the codebook become effectively decoupled. Consequently, the codebook vectors fail to adaptively track the distribution of semantic features. To jointly optimize the encoder and the semantic codebook while ensuring the stability of the discretization process, we introduce a quantization regularization loss \mathcal{L}_{quant} defined as follows:

$$\mathcal{L}_{quant}(\boldsymbol{\theta}) = \mathbb{E}_{p(\mathbf{X})} \left[\|\text{sg}[\mathbf{L}] - \mathbf{L}_{vq}\|_2^2 + \beta_q \|\mathbf{L} - \text{sg}[\mathbf{L}_{vq}]\|_2^2 \right], \quad (24)$$

where $\text{sg}[\cdot]$ denotes the stop-gradient operator, which blocks gradient propagation during backpropagation, \mathbf{L}_{vq} represents the semantically meaningful representation after vector quantization, and β_q is a hyperparameter that balances the contributions of the two loss terms.

The first term in equation (24) is designed to drive the learning of the codebook. By applying $\text{sg}[\mathbf{L}]$, this term computes gradients only with respect to the codebook, forcing the selected embedding vectors to move toward the current encoder outputs. The second term acts as a regularization constraint on the encoder. By freezing the codebook vectors via $\text{sg}[\mathbf{L}_{vq}]$, this term encourages the encoder to generate feature representations that remain close to their corresponding quantization centers, thereby effectively limiting quantization error.

Although \mathcal{L}_{quant} does not directly measure the quality of semantic reconstruction, it serves as a structural constraint imposed on the variational posterior distribution. By enforcing topological consistency between the continuous semantic space and the discrete symbol space, this regularization provides a crucial foundation for the stable convergence of the entire end-to-end system.

In practical computations, the probability distribution is replaced by the empirical distribution according to the law of large numbers, leading to the loss function in (21). Based on the above analysis, the training algorithm of the proposed SFSC scheme is summarized in Algorithm 1. To accelerate training, a pretrained vector quantized variational autoencoder (VQ-VAE) [44] model is first loaded to initialize the semantic encoder, decoder and the semantic codebook. VQ-VAE learns a discrete latent feature that aligns with the digital semantic codebook employed in our system. Therefore, utilizing a pretrained VQ-VAE model provides a high-quality shared codebook for both the transmitter and receiver, enabling the semantic encoder to extract semantic features with high fidelity at the initial stage of end-to-end training. Then, a mini-batch of samples is drawn from the training dataset

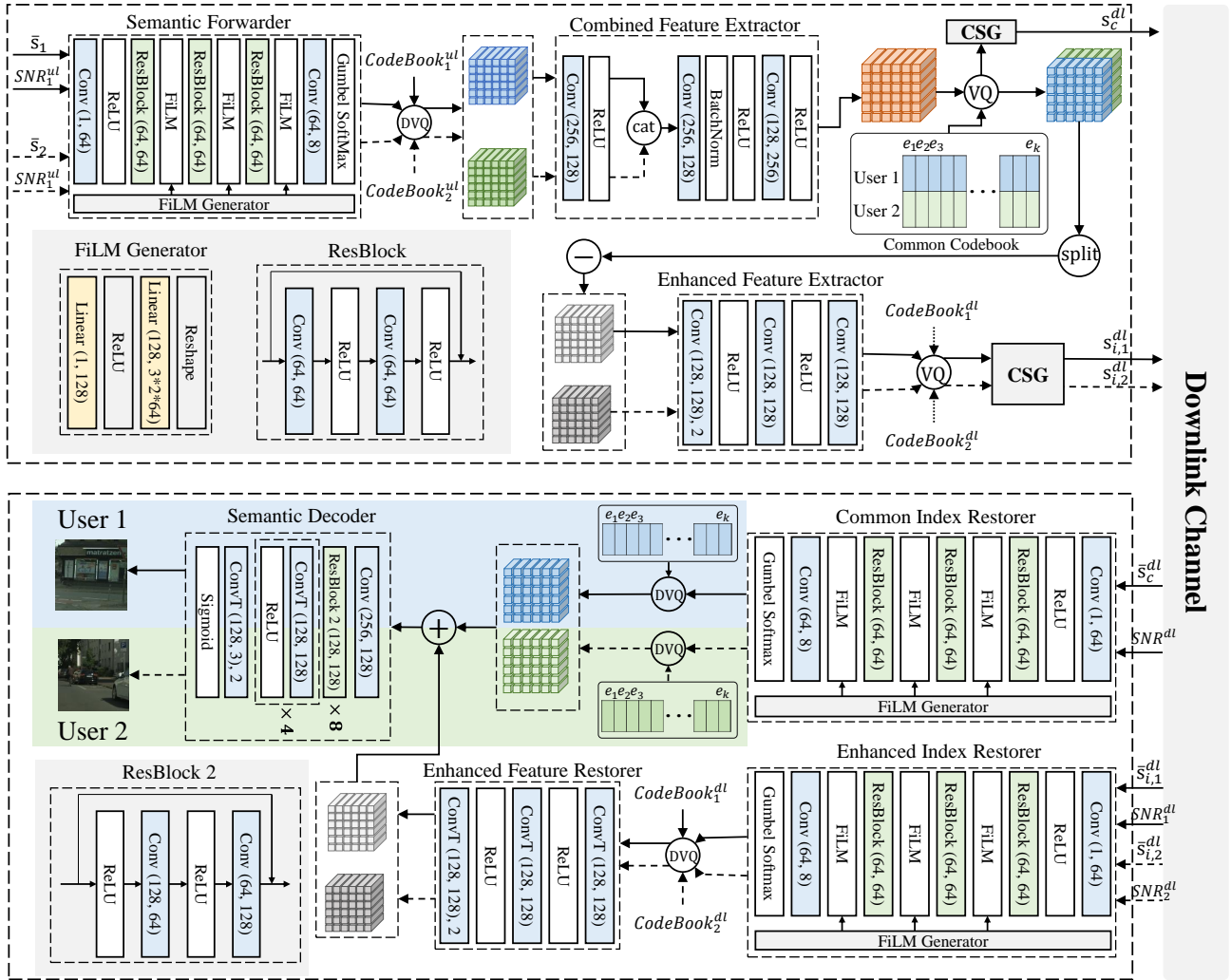


Fig. 4: Framework of downlink CS-MDMA transmission from the satellite relay node to the ground receivers, with detailed neural network structures presented. It illustrates the satellite relay node employing the common orthogonal codebook to produce common signals, and deriving private signals via the enhanced feature extractor. At the receiver, the index restorers and enhanced feature restorers cooperatively recover the latent semantic features for high-fidelity decoding.

and encoded by the semantic encoder to obtain semantic features. These semantic features are subsequently vector-quantized, and the ReinMax method is employed to generate differentiable constellation symbols followed by power normalization. After transmission over the service uplink channel, the satellite relay node performs semantic forwarding on the received signals via the semantic forwarder to generate the feeder downlink transmit signals. After propagation through the feeder downlink channel, the ground receiver first recovers the required codebook indexes using the index restorer. Based on the semantic codebook shared between the transmitter and the receiver, the semantic features are then recovered and fed into the semantic decoder to reconstruct the image information. Finally, the loss function is computed, and the model parameters are iteratively updated using gradient descent.

III. CODEBOOK SPLIT-ENHANCED MDMA APPROACH

In this section, we provide a detailed description of the proposed CS-MDMA approach. The approach consists of the

encoding-modulation process at the UT nodes, the relay forwarding, superposition coding, and information enhancement processes at the satellite relay node, as well as the data recovery process at the ground receiver node. Since the UT encoding-modulation process is similar to that presented in Section II-B, our focus here is on the feeder downlink transmission from the satellite relay to the ground receiver. Fig. 4 illustrates the downlink CS-MDMA transmission framework from the satellite relay node to the ground receivers.

The proposed scheme employs a common orthogonal codebook to perform superposition coding on semantic information, enabling the simultaneous transmission of information from multiple users within the same resource block. This design improves bandwidth utilization efficiency and improves data transmission quality in satellite communication systems.

A. Codebook Split and Superposition Coding Technique

As shown in Fig. 4, the information from the two user terminals is transformed into one-hot vector-quantized indices

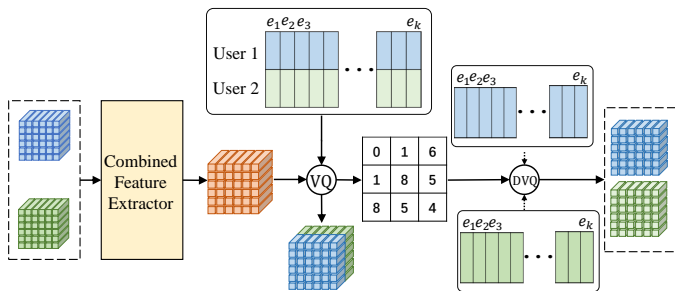


Fig. 5: Illustration of the process of codebook split. A common orthogonal codebook is divided into disjoint user-specific sub-codebooks. This enables the system to map combined features to unique indices and decouple them into private semantics.

based on their respective VQ-PEM modules and private codebooks. These indices are then converted by the CSG into transmitted complex signals s_1 and s_2 , which serve as the channel input. The corresponding signals received at the satellite relay node are denoted by \bar{s}_1 and \bar{s}_2 .

Through the semantic forwarder deployed at the satellite relay node, the recovered one-hot indices are expressed as

$$\bar{\mathbf{I}}_k = f_{sf}(\bar{s}_k; \boldsymbol{\theta}_{sf}). \quad (25)$$

Based on the recovered one-hot indices and the semantic codebook \mathbf{E}_k of the two users, the reconstructed quantized semantic features are given by

$$\bar{\mathbf{L}}_k = \text{VDQ}(\bar{\mathbf{I}}_k, \mathbf{E}_k), \quad (26)$$

where $\text{VDQ}(\cdot, \mathbf{E}_k) = \text{matmul}(\cdot, \mathbf{E}_k)$ denotes the matrix multiplication operation and $k \in \{1, 2\}$.

As shown in Fig. 5, to enable the propagation of different users' information within the same codebook space, inspired by MDMA technique, we design a new codebook referred to as the common orthogonal codebook

$$\mathbf{E}_c = [\mathbf{e}_1, \mathbf{e}_2, \dots, \mathbf{e}_K]^T \in \mathbb{R}^{K \times (P_1 + P_2)}, \quad (27)$$

where $\mathbf{e}_k = \text{concat}(\mathbf{e}_k^{p_1}, \mathbf{e}_k^{p_2}) \in \mathbb{R}^{(P_1 + P_2) \times 1}$, $\mathbf{e}_k^{p_1} \in \mathbb{R}^{P_1 \times 1}$ and $\mathbf{e}_k^{p_2} \in \mathbb{R}^{P_2 \times 1}$ denote the feature segments corresponding to user 1 and user 2, respectively, with $k \in \{1, \dots, K\}$.

A combined feature extractor is then employed to combine the reconstructed quantized semantic features of the two users. It extracts a combined semantic representation and aligns its dimensionality with that of the common orthogonal codebook

$$\mathbf{L}_{combine} = f_{cfe}(\bar{\mathbf{L}}_1, \bar{\mathbf{L}}_2; \boldsymbol{\theta}_{cfe}), \quad (28)$$

where $f_{cfe}(\cdot; \boldsymbol{\theta}_{cfe})$ denotes the feature combine encoder with learnable parameters $\boldsymbol{\theta}_{cfe}$, and $\mathbf{L}_{combine} = [\mathbf{l}_1, \mathbf{l}_2, \dots, \mathbf{l}_M]^T \in \mathbb{R}^{M \times (P_1 + P_2)}$, with M representing the number of feature vectors.

Based on the common orthogonal codebook, vector quantization is applied to the combined semantic features, enabling the separation of user-specific private information across the feature-channel dimension and simultaneous transmission over the same resource

$$\mathbf{k}_{combine} = \text{VQ}(\mathbf{L}_{combine}; \mathbf{E}_c), \quad (29)$$

where $\mathbf{k}_{combine} = [k_1, k_2, \dots, k_M] \in \mathbb{R}^M$, $k_m = \text{argmin}_m \|\mathbf{l}_m - \mathbf{e}_k\|$, and its one-hot representation is $\mathbf{I}_{combine} = [\mathbf{i}_1, \mathbf{i}_2, \dots, \mathbf{i}_M]^T \in \mathbb{R}^{M \times K}$, where each \mathbf{i}_m is a one-hot vector with the k_m -th element being 1, $m \in [1, M]$, $k \in [1, K]$.

By splitting the common orthogonal codebook, the semantic information of user 1 and user 2 is obtained as

$$\bar{\mathbf{L}}_u^{split} = \text{matmul}(\mathbf{I}_{combine}, \mathbf{E}_c^u), \quad (30)$$

where $\mathbf{E}_c^u = [\mathbf{e}_1^{p_u}, \mathbf{e}_2^{p_u}, \dots, \mathbf{e}_K^{p_u}]^T \in \mathbb{R}^{K \times P_u}$ denotes the sub-codebook, with $u \in \{1, 2\}$.

Finally, the feeder downlink transmitted complex signal s_c^{dl} is generated through the constellation symbol generator and used as the channel input.

B. Private Information Enhance

Through the above superposition encoding defined by equations (28)-(30), the semantic information of different users is encoded into the same transmitted signal s_c^{dl} . Although the codebook split strategy enables the simultaneous transmission of multiple users' information while preserving the separation of their private semantics, it inevitably introduces feature distortion. This distortion can be attributed to the superposition of semantic information among different users. According to the analysis in Section II, we assume that the overall reconstruction loss can be expressed as

$$\begin{aligned} \mathcal{L}_u^{recon} &= \mathbb{E} \|\mathbf{X}_u - f_{de}(\bar{\mathbf{L}}_u^{split})\|_2^2 \\ &= \mathbb{E} \|\boldsymbol{\varepsilon}_u^{\text{in}} + \boldsymbol{\varepsilon}_u^{\text{sup}}\|_2^2 \\ &= \mathbb{E} \|\boldsymbol{\varepsilon}_u^{\text{in}}\|_2^2 + \mathbb{E} \|\boldsymbol{\varepsilon}_u^{\text{sup}}\|_2^2 + 2\mathbb{E} \left[(\boldsymbol{\varepsilon}_u^{\text{in}})^T \boldsymbol{\varepsilon}_u^{\text{sup}} \right], \end{aligned} \quad (31)$$

where $f_{de}(\cdot)$ denotes the ideal reconstruction function, $\boldsymbol{\varepsilon}_u^{\text{in}} \triangleq \mathbf{X}_u - f_{de}(\bar{\mathbf{L}}_u)$ denotes the intrinsic reconstruction error, $\boldsymbol{\varepsilon}_u^{\text{sup}} \triangleq f_{de}(\bar{\mathbf{L}}_u) - f_{de}(\bar{\mathbf{L}}_u^{split})$ denotes the superposition residual captured by the origin features relative to the split features. The first term represents the reconstruction capability limit of the original semantic coder, while the third term corresponds to the cross term between the inherent reconstruction error of the original semantic information and the additional error due to superposition encoding. To facilitate the analysis, we statistically assume that the additional error is uncorrelated with the inherent reconstruction error, such that the expectation of this cross term approaches zero. Consequently, by applying a first-order Taylor expansion, the superposition loss caused by multi-user semantic information superposition can be approximated as

$$\begin{aligned} \mathcal{L}_u^{superpose} &= \mathbb{E} \|(f_{de}(\bar{\mathbf{L}}_u) - f_{de}(\bar{\mathbf{L}}_u^{split}))\|_2^2 \\ &\approx \mathbb{E} \|J_{f_{de}}(\bar{\mathbf{L}}_u) \mathbf{r}\|_2^2 \\ &= \mathbb{E} (\mathbf{r}^T \mathbf{M} \mathbf{r}), \end{aligned} \quad (32)$$

where $J_{f_{de}}(\bar{\mathbf{L}}_u)$ denotes the Jacobian matrix of $f_{de}(\cdot)$ evaluated at $\bar{\mathbf{L}}_u$, and $\mathbf{M} = J_{f_{de}}(\bar{\mathbf{L}}_u)^T J_{f_{de}}(\bar{\mathbf{L}}_u)$ is a positive semi-definite matrix that characterizes the sensitivity of the decoder along different directions in the feature space. Therefore, to ensure high-quality image reconstruction, inspired by classical MDMA schemes, we further propose a semantic

information enhancement mechanism based on codebook split. The enhanced semantic representation is given by

$$\bar{\mathbf{L}}_u^{enhance} = f_{efe}(\bar{\mathbf{L}}_u - \bar{\mathbf{L}}_u^{Split}; \boldsymbol{\theta}_{efe}), \quad (33)$$

where $f_{efe}(\cdot; \boldsymbol{\theta}_{efe})$ denotes the enhanced feature extractor with trainable parameters $\boldsymbol{\theta}_{efe}$. The enhanced feature extractor learns to compress the feature residual by using the positive semi-definite matrix M that characterizes the decoder sensitivity, with $u \in \{1, 2\}$. After quantization and modulation, the enhanced semantic representation $\bar{\mathbf{L}}_u^{enhance}$ is mapped into the enhanced semantic signal $\mathbf{s}_{i,u}^{dl}$.

C. Codebook Split-enhanced Semantic Recovery

Similarly to Section II, the ground receivers first process the downlink signals through their corresponding index restorers. Through this module, each user obtains the one-hot information indices $\hat{\mathbf{I}}^{combine}$, $\hat{\mathbf{I}}_1^{enhance}$ or $\hat{\mathbf{I}}_2^{enhance}$, which respectively represent the combined information indices decoded from the common downlink signal and the enhanced indices decoded from the individual enhanced signals. These decoded indices serve as the discrete semantic identifiers required for subsequent de-quantization, enabling each user to retrieve the semantic features carried in both the common and enhanced branches. Based on these indices, receivers further obtain the enhanced semantic information $\hat{\mathbf{L}}_1^{enhance}$ and $\hat{\mathbf{L}}_2^{enhance}$.

In particular, as described in Section III-A, splitting the common orthogonal codebook yields the user-specific sub-codebooks \mathbf{E}_c^1 and \mathbf{E}_c^2 . These sub-codebooks contain the feature segments that correspond to the semantic subspace allocated to each user. By leveraging their own sub-codebook, each user de-quantizes the decoded combined information indices to obtain its latent semantic feature, which is formulated as

$$\hat{\mathbf{L}}_u^{split} = \text{matmul}(\hat{\mathbf{I}}^{combine}, \mathbf{E}_c^u). \quad (34)$$

This operation ensures that the user can correctly reconstruct the semantic feature originally mapped to the common orthogonal codebook space while maintaining user-specific separability across the feature-channel dimension. For the enhanced semantic information, each user employs an enhanced feature restorer to reconstruct the residual semantic feature that is introduced to mitigate the superposition loss of the shared codebook. The reconstructed residual semantic feature is given by

$$\hat{\mathbf{L}}_u^{res} = f_{efr}(\hat{\mathbf{L}}_u^{enhance}; \boldsymbol{\theta}_{efr}), \quad (35)$$

where $f_{efr}(\cdot; \boldsymbol{\theta}_{efr})$ denotes the enhanced feature restorer with learnable parameters $\boldsymbol{\theta}_{efr}$. This component plays a crucial role in restoring fine-grained semantic details that are partially lost during superposition coding and vector quantization.

Consequently, the final recovered semantic representation for each user is obtained by combining the reconstructed latent semantic component with the reconstructed residual component

$$\hat{\mathbf{L}}_u = \hat{\mathbf{L}}_u^{split} + \hat{\mathbf{L}}_u^{res}. \quad (36)$$

This reconstructed latent semantic feature captures both the global structural content and the user-specific refinements required for high-fidelity reconstruction.

Algorithm 2: CS-MDMA enhanced SFSC Training Algorithm

Initialization: Initialize the model parameters $\boldsymbol{\theta}$, training dataset \mathcal{D} , epoch number E and batch size B .

for $t = 1$ **to** E **do**

Select mini-batch data $\{\mathbf{X}_1, \mathbf{X}_2\}_{i=n}^{n+B}$ from \mathcal{D}

for $k = 1$ **to** 2 **do**

Satellite uplink transmission:

$$\{\mathbf{X}_k\}_{i=n}^{n+B} \longrightarrow \{\bar{\mathbf{s}}_k\}_{i=n}^{n+B}$$

Satellite relay recovery:

$$\{\bar{\mathbf{s}}_k\}_{i=n}^{n+B} \xrightarrow{f_{sf}(\cdot; \boldsymbol{\theta})} \{\bar{\mathbf{I}}_k\}_{i=n}^{n+B} \xrightarrow{\mathcal{V}^{DQ}} \{\bar{\mathbf{L}}_k\}_{i=n}^{n+B}$$

CS-MDMA coding:

$$\{\bar{\mathbf{L}}_1, \bar{\mathbf{L}}_2\}_{i=n}^{n+B} \xrightarrow{f_{cs}(\cdot; \boldsymbol{\theta})} \{\mathbf{s}_c^{dl}, \mathbf{s}_{e,1}^{dl}, \mathbf{s}_{e,2}^{dl}\}_{i=n}^{n+B}$$

Satellite downlink channel:

$$\{\mathbf{s}_c^{dl}, \mathbf{s}_{e,1}^{dl}, \mathbf{s}_{e,2}^{dl}\}_{i=n}^{n+B} \longrightarrow \{\hat{\mathbf{s}}_c^{dl}, \hat{\mathbf{s}}_{e,1}^{dl}, \hat{\mathbf{s}}_{e,2}^{dl}\}_{i=n}^{n+B}$$

Latent feature recovery:

$$\{\hat{\mathbf{s}}_c^{dl}\}_{i=n}^{n+B} \xrightarrow{f_{cir}(\cdot; \boldsymbol{\theta})} \{\hat{\mathbf{I}}_c\}_{i=n}^{n+B},$$

$$\{\hat{\mathbf{I}}_c\}_{i=n}^{n+B} \xrightarrow{\mathbf{E}_c^1, \mathbf{E}_c^2} \{\hat{\mathbf{L}}_1^{split}, \hat{\mathbf{L}}_2^{split}\}_{i=n}^{n+B}$$

for $k = 1$ **to** 2 **do**

Enhanced feature recovery:

$$\{\hat{\mathbf{s}}_{e,k}^{dl}\}_{i=n}^{n+B} \xrightarrow{f_{eir}(\cdot; \boldsymbol{\theta})} \{\hat{\mathbf{I}}_{e,k}\}_{i=n}^{n+B},$$

$$\{\hat{\mathbf{I}}_{e,k}\}_{i=n}^{n+B} \xrightarrow{\mathcal{V}^{DQ}, f_{efr}(\cdot; \boldsymbol{\theta})} \{\hat{\mathbf{L}}_{e,k}\}_{i=n}^{n+B}$$

Semantic feature recovery:

$$\{\hat{\mathbf{L}}_k\}_{i=n}^{n+B} = \{\hat{\mathbf{L}}_k^{split}\}_{i=n}^{n+B} + \{\hat{\mathbf{L}}_{e,k}\}_{i=n}^{n+B}$$

Semantic decoding:

$$\{\hat{\mathbf{L}}_k\}_{i=n}^{n+B} \xrightarrow{f_{sd}(\cdot; \boldsymbol{\theta})} \{\hat{\mathbf{X}}_k\}_{i=n}^{n+B}$$

Compute loss $\mathcal{L}(\boldsymbol{\theta})$

Update $\boldsymbol{\theta}$ through gradient descent with $\mathcal{L}(\boldsymbol{\theta})$

return Trained parameters $\boldsymbol{\theta}$

Similarly to Section II, the final reconstructed image is produced through the semantic decoder, which transforms the recovered semantic representation into the pixel domain

$$\hat{\mathbf{X}}_u = f_{sd}(\hat{\mathbf{L}}_u; \boldsymbol{\theta}_{sd}). \quad (37)$$

The semantic decoder, parameterized by $\boldsymbol{\theta}_{sd}$, ensures that the reconstructed images maintain consistency with the original content while benefiting from the compact and structure-aware representation enabled by the proposed CS-MDMA framework. Based on the above discussion, the training process of the proposed CS-MDMA enhanced SFSC scheme is summarized in Algorithm 2.

IV. SIMULATION AND RESULTS

A. Performance Benchmarks and Evaluation Metric

To objectively evaluate the performance advantages of the proposed SFSC scheme and CS-MDMA enhanced SFSC scheme, we compare them with several baseline methods operating under different relay modes: 1) Analog semantic transmission based on DeepJSCC [20]; according to the processing capability of the satellite relay node, this scheme is further divided into two modes. In the transparent mode

TABLE II: SYSTEM NETWORK STRUCTURE PARAMETERS

Module	Layer Structure
Semantic Encoder f_{se} $3 \times 512 \times 512 - 256 \times 256 \times 256$	Conv2d (3,128,4,2,1)
	Conv2d (128,128,3,1,1)
	ResBlock (128,128) $\times 2$
	Conv2d (128,256,1,1)
Vector Quantizer f_{vq} $256 \times 256 \times 256 - 256 \times 256 \times 8$	Embedding (8, 256)
Semantic Forwarder f_{sf} $1 \times 256 \times 256 - 8 \times 256 \times 256$	Conv2d (1,64,3,1,1)
	ResBlock (64, 64)
	FiLM
	ResBlock (64, 64)
	FiLM
	ResBlock (64, 64)
	FiLM
	Conv2d (64,8,1,1)
Index Restorer f_{ir} $1 \times 256 \times 256 - 8 \times 256 \times 256$	Conv2d (1,64,3,1,1)
	ResBlock (64, 64)
	FiLM
	ResBlock (64, 64)
	FiLM
	ResBlock (64, 64)
	FiLM
	Conv2d (64,8,1,1)
FiLM Generator f_g $3 \times 256 \times 256 - 128 \times 256 \times 256$	Conv2d (3,128,3,1,1)
	Conv2d (128,128,3,1,1)
	Conv2d (128,128,1,1)
	Conv2d (256,128,1,1)
Semantic Decoder f_{sd} $256 \times 256 \times 256 - 3 \times 512 \times 512$	ResBlock (128,128) $\times 2$
	ConvT (128,128,3,1,1)
	ConvT (128,3,4,2,1)

(TM-DeepJSCC), the ground receiver directly processes a composite signal corrupted by the noise from both the uplink and downlink. In contrast, in the regenerative mode (RM-DeepJSCC), the satellite adopts a decode-and-forward strategy, where semantic features are reconstructed and re-encoded on-board to mitigate the interference introduced by the uplink channel. 2) Digital semantic transmission based on joint coding and modulation [28] (JCM): similarly, depending on the on-board processing strategy, this approach is categorized into transparent mode JCM (TM-JCM) and regenerative mode JCM (RM-JCM), enabling an assessment of the adaptability of digital semantic transmission mechanisms over satellite relay channels. 3) Traditional source-channel separation scheme: This classical approach employs JPEG for image source coding in conjunction with low-density parity-check (LDPC) codes for channel coding. To comprehensively evaluate SFSC scheme against the baseline, we consider two representative configurations that capture distinct trade-offs between compression rate of JPEG and bit error rate of LDPC, while maintaining a transmission rate of approximately $\frac{1}{12}$. The first configuration compresses the source image to approximately 84 Kbits using JPEG and applies an LDPC code with a rate

of 3072/4608, thereby prioritizing source fidelity. The second configuration further reduces the source size to 64 Kbits, while adopting a more robust LDPC code rate of 2304/4608 to enhance transmission reliability. Both configurations employ 4-QAM modulation and result in a comparable total number of transmitted symbols.

To demonstrate the performance advantages of the CS-MDMA enhanced SFSC scheme over satellite relay links, particularly in the downlink transmission, we adopt a full satellite relay link in the simulations of the CS-MDMA enhanced SFSC scheme. In contrast, for the baseline schemes, we assume ideal information recovery over the uplink, thereby focusing the comparison on downlink multi-access transmission. We consider the following baseline schemes: 1) MDMA transmission [23]: A classical model division multiple access scheme is employed, with a DeepJSCC model used as the semantic encoder and decoder, and analog transmission is adopted. Both users employ the same semantic encoder to extract semantic representations, which are then processed by the MDMA module to obtain shared and personalized features. These features are transmitted to the ground receiver, where the shared and personalized information is combined and fed into the same semantic decoder to reconstruct the image content. 2) NOMA transmission: NOMA is employed with binary phase shift keying (BPSK) modulation, and a VQ-VAE [44] model trained under noise-free conditions is used as the semantic encoder. In the two-user multiple-access scenario, the power allocation factors for the users are set to 0.9 and 0.1, respectively. 3) JSCC-trained NOMA transmission (NOMA-JSCC): NOMA is combined with BPSK modulation, and a VQ-VAE model trained over a bit-flip channel is adopted as the semantic encoder. In the two-user multiple-access scenario, the power allocation factors for the users are also set to 0.9 and 0.1, respectively.

We employ classical image reconstruction quality metrics to evaluate and compare the performance of the proposed schemes.

1) *Peak Signal-to-Noise Ratio (PSNR)*: PSNR is a standardized metric for evaluating the quality of lossy image reconstruction, which primarily measures the distortion level by computing the pixel-wise error between the original image and the reconstructed image. A higher PSNR value indicates a smaller mean squared error (MSE) between the reconstructed image and the original image, and thus better reconstruction quality. Its mathematical definition is given by

$$\text{PSNR}[dB] = 10 \log_{10} \left(\frac{\text{MAX}^2}{\text{MSE}} \right), \quad (38)$$

where MAX denotes the maximum possible pixel value of the image. The MSE represents the mean squared error between the original image and the reconstructed image, defined as

$$\text{MSE} = \frac{1}{L_x} \|\mathbf{X} - \hat{\mathbf{X}}\|_2^2, \quad (39)$$

where L_x is the dimensionality of the input image.

2) *Multi-Scale Structural Similarity (MS-SSIM)*: The conventional structural similarity index (SSIM) evaluates perceptual image quality by jointly considering luminance, contrast,

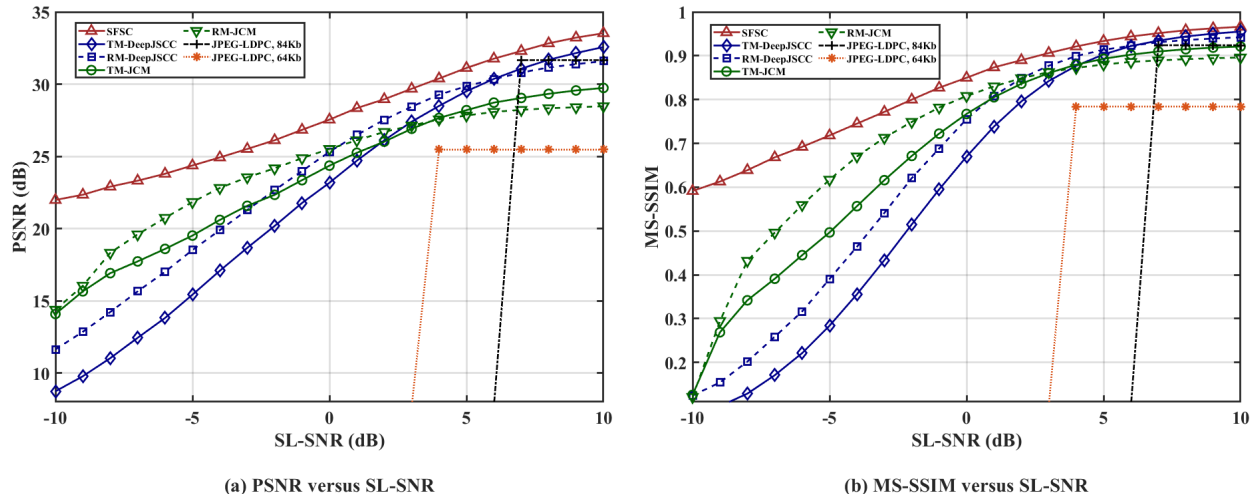


Fig. 6: Performance evaluation of SFSC and baselines in terms of (a) PSNR, (b) MS-SSIM metrics versus SL-SNRs in satellite relay channel.

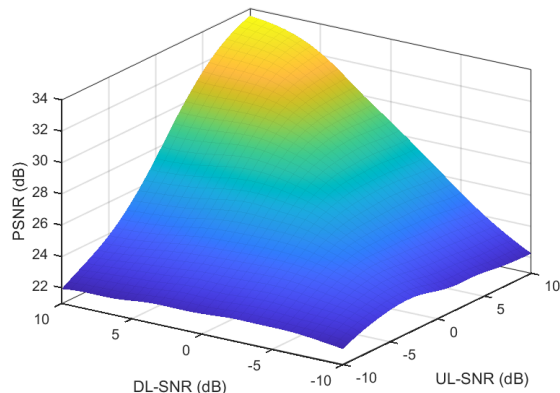


Fig. 7: PSNR estimation surface for SFSC versus UL-SNR and DL-SNR in satellite relay channel.

and structural information [55]. However, to more effectively capture image details under different resolutions and viewing conditions, we adopt MS-SSIM [56]. Building upon SSIM, MS-SSIM performs multiple stages of downsampling and assesses structural similarity across multiple scales. Its formulation is given by

$$\text{MS-SSIM}(\mathbf{X}, \hat{\mathbf{X}}) = [l_M(\mathbf{X}, \hat{\mathbf{X}})]^{\alpha_M} \cdot \prod_{j=1}^M [c_j(\mathbf{X}, \hat{\mathbf{X}})]^{\beta_j} [s_j(\mathbf{X}, \hat{\mathbf{X}})]^{\gamma_j}, \quad (40)$$

where l_M denotes the luminance comparison component at the coarsest scale, while c_j and s_j represent the contrast and structural comparison components at the j -th scale, respectively. The exponents α_M , β_j , and γ_j are weighting factors that control the relative importance of each component. The MS-SSIM metric ranges from $[0, 1]$, with values closer to 1 indicating higher perceptual similarity between the reconstructed and original images across multiple scales.

To quantify the transmission rate, we define it as the ratio between the number of channel uses and the dimensionality

of the image data [28]. For an image of size $512 \times 512 \times 3$, the transmission rate is given by

$$r = \frac{n}{512 \times 512 \times 3}, \quad (41)$$

where n denotes the number of channels used. For example, in the SFSC system network architecture illustrated in Table II, the transmission rate is $\frac{1}{24}$.

B. Experimental Settings and Dataset

We consider a satellite relay system based on semantic communications, which follows the frequency-selective fading tapped delay line (NTN-TDL-D) channel model as specified in 3GPP TR 38.811 [11]. Within this framework, the UT transmits the encoded image semantic information to a regenerative satellite via the uplink. After performing semantic forwarding on-board, the satellite forwards the processed signal to the ground gateway.

In the simulations, the detailed network architecture parameters of the SFSC scheme are summarized in Table II. In the first column, below each model module name are the input and output sizes of the modules. The parameters in brackets in the second column represents parameters (in channels, out channels, kernel size, stride, and padding). In addition, the CS-MDMA enhanced SFSC adopts the same transmitter architecture as the baseline SFSC, while the architectures of the satellite relay and the ground receiver are illustrated in Fig. 4.

The experiments are conducted using the Cityscapes dataset for model training and evaluation [57]. The dataset consists of 2,975 training images, 500 validation images, and 1,525 test images. All images from the Cityscapes dataset are downsampled to 512×512 before being fed into the model. The proposed model is optimized using the Adam optimizer, and the entire training process is carried out on two NVIDIA A10 GPUs.

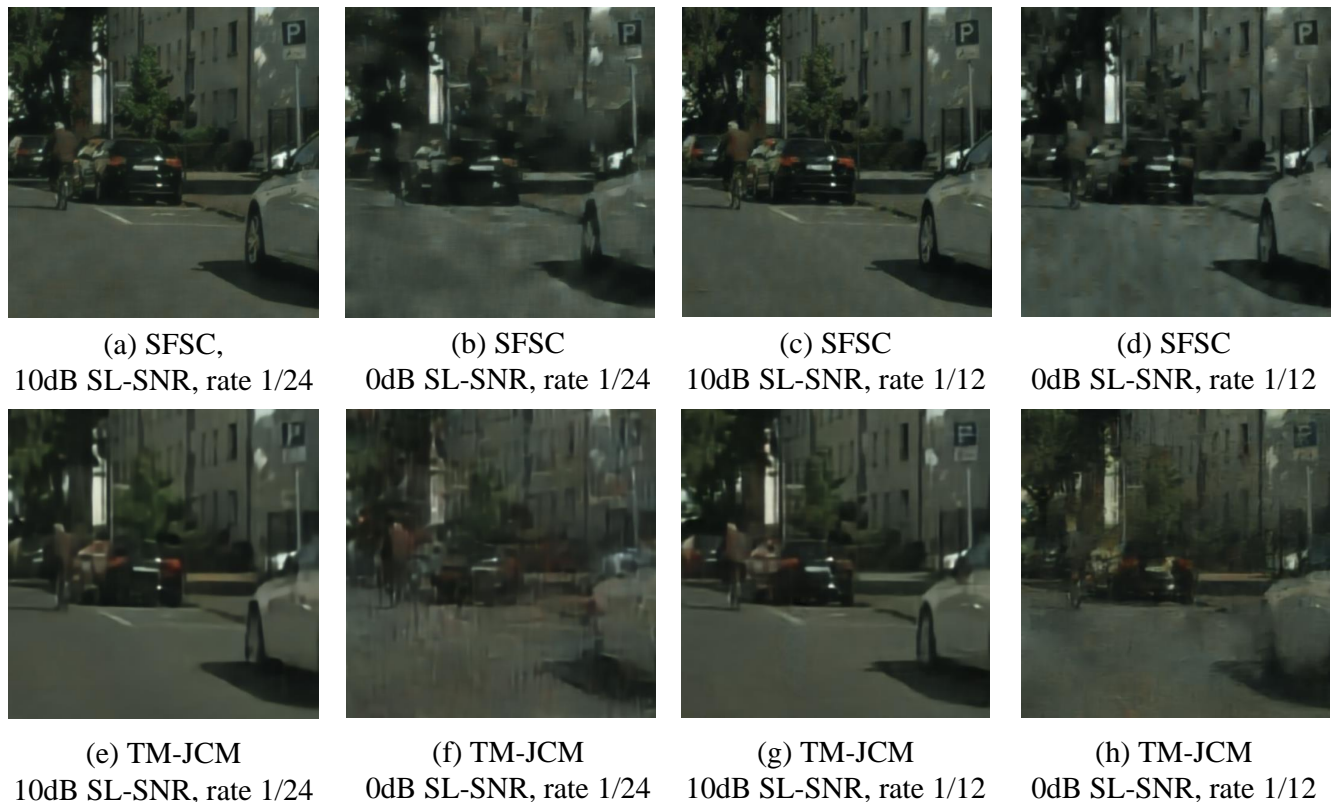


Fig. 8: Image examples restored by the competing methods under different transmission scenarios.

C. Results and Analysis

To facilitate a fair comparative analysis, we assume that the SNR of the source-to-relay link (UL-SNR) and that of the relay-to-destination link (DL-SNR) are identical, and denote them collectively as the single-link SNR (SL-SNR). Fig. 6 presents the performance comparison between the proposed SFSC scheme and the baseline methods over satellite relay channels with SL-SNR ranging from -10 dB to 10 dB. In this comparison, the digital semantic transmission schemes operate at a transmission rate of $\frac{1}{24}$ and employ 64-QAM modulation, while the analog transmission schemes use a transmission rate of $\frac{1}{32}$. As shown in Fig. 6(a), under an extremely low SL-SNR of -10 dB, the proposed SFSC scheme achieves PSNR gains of 7.893 dB and 13.249 dB over the transparent-mode TM-JCM and TM-DeepJSCC schemes, respectively, demonstrating its strong robustness under severe channel conditions. At a lower SL-SNR of 0 dB, although the PSNR gaps among different schemes are reduced, SFSC still outperforms the above two schemes by 3.184 dB and 4.371 dB, respectively. When the SL-SNR increases to 10 dB, SFSC continues to exhibit performance advantages, achieving PSNR gains of 3.789 dB and 0.957 dB over the two baseline schemes, which highlights its efficient transmission capability. Furthermore, the proposed SFSC scheme effectively mitigates the “cliff effect” that typically plagues traditional digital transmission frameworks.

Regenerative-mode TM-DeepJSCC and TM-JCM mitigate noise accumulation under harsh satellite relay channel condi-

tions by performing semantic decoding and re-encoding at the satellite relay node. As a result, compared with their transparent-mode counterparts, regenerative schemes achieve superior performance in the low SNR regime. However, at high SL-SNR levels, the impact of channel impairments on image reconstruction quality becomes less dominant, while the semantic noise introduced by on-board semantic encoding and decoding at the satellite relay becomes more pronounced, making transparent-mode schemes more advantageous in this regime.

Unlike regenerative approaches, SFSC does not perform full semantic decoding and re-encoding at the satellite relay. Instead, it realizes semantic forwarding by learning the prior distribution of the transmitted signals and the constellation transition probabilities of the uplink channel. This design both alleviates noise accumulation and avoids the introduction of additional semantic noise. Consequently, the proposed SFSC scheme consistently outperforms the baseline methods across the entire SL-SNR range.

Fig. 6(b) presents the SSIM performance comparison between the proposed SFSC scheme and the baseline methods. Similar to the observations in Fig. 6(a), SFSC consistently outperforms all baseline schemes across the entire SL-SNR range, with particularly pronounced gains in the low SL-SNR regime, further validating the robustness of the proposed approach over satellite relay channels.

To investigate the impact of asymmetric uplink and downlink channel qualities on the performance of SFSC, Fig. 7 depicts the PSNR performance of the SFSC scheme under

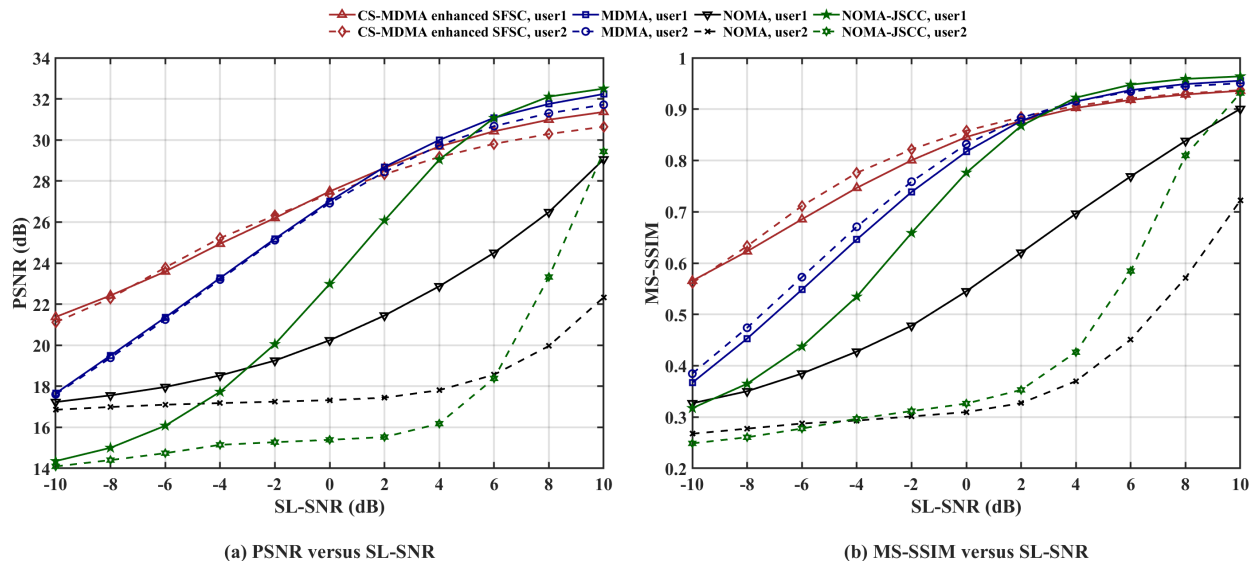


Fig. 9: Performance evaluation of CS-MDMA enhanced SFSC and baselines in terms of (a) PSNR, (b) MS-SSIM metrics versus SL-SNRs in satellite relay channel.

different combinations of UL-SNR and DL-SNR. It can be observed that, under the same overall noise level, the uplink channel quality has a more pronounced influence on the final image reconstruction quality than the downlink channel quality. Specifically, when setting (UL-SNR, DL-SNR) to (10, 4), the achieved PSNR is 0.627 dB (2.0%) higher than that obtained with (4, 10). Similarly, the PSNR under (6, 0) exceeds that under (0, 6) by 1.194 dB (4.3%). We attribute this difference to the unavoidable noise amplification incurred during satellite relaying. Although the uplink and downlink channel qualities exhibit slightly different impacts on the final reconstruction performance, the difference is not substantial. Therefore, we conclude that the effects of UL-SNR and DL-SNR on the SFSC performance are approximately symmetric. That is, when one link SNR is fixed, the PSNR shows a similar growth trend as the channel quality of the other link improves. This observation validates the reasonableness of the single-link SNR assumption adopted in our analysis.

The visual comparisons in Fig. 8 clearly illustrate the differences between the proposed SFSC scheme and the TM-JCM scheme. Under high-SNR conditions, SFSC reconstructs images with sharper edges and preserves fine details more effectively. As the noise level increases, the main content of the images processed by TM-JCM becomes severely degraded. In contrast, the performance degradation of SFSC mainly manifests as the loss of global or local details, such as color and texture, while the semantic content of the scene remains clearly identifiable, including objects such as cars, cyclists, and traffic signs shown in the figure.

These observations indicate that, in the SFSC scheme, the learning-based semantic forwarding mechanism effectively suppresses noise accumulation. Moreover, channel-aware adaptive semantic forwarding and information recovery enhance the overall system robustness. In addition, the VQ-based probabilistic encoder-modulator is better at capturing the global semantic structure of images than the probabilistic

encoder-modulator employed in JCM, further contributing to the superior performance of SFSC.

Fig. 9 presents the performance comparison between the CS-MDMA enhanced SFSC scheme and the baseline methods over satellite relay channels with SL-SNR ranging from -10 dB to 10 dB. In the CS-MDMA enhanced SFSC scheme, the same uplink transmitter model as that of SFSC is adopted, with a single-user uplink transmission rate of $\frac{1}{24}$. After semantic forwarding and CS-MDMA processing at the satellite relay, the signals are encoded into a CS-MDMA downlink signal with a transmission rate of $\frac{1}{48}$ for two users and two enhancement signals with a transmission rate of $\frac{1}{96}$ for two users, both employing 64-QAM modulation.

For the classical MDMA scheme, the satellite performs semantic encoding and MDMA processing, generating a shared signal with a transmission rate of $\frac{1}{64}$ for two users and two personalized signals with a transmission rate of $\frac{1}{32}$ for two users. The NOMA and NOMA-JSCC schemes both adopt a VQ-VAE model as the semantic encoder and decoder, with a single-user transmission rate of $\frac{1}{32}$.

As shown in Fig. 9(a), at relatively high SL-SNR values, the CS-MDMA enhanced SFSC achieves performance comparable to that of the MDMA and NOMA-JSCC schemes. In contrast, at low SL-SNR, the CS-MDMA enhanced SFSC significantly outperforms both MDMA and NOMA-JSCC, achieving a PSNR gain of 4.49-7.02 dB over all baseline methods at -10 dB.

The NOMA scheme suffers from limited performance due to the lack of effective channel coding. In particular, the low-power user heavily relies on the correct demodulation of the high-power user. Although the NOMA-JSCC scheme alleviates the impact of demodulation errors through JSCC-based training, its performance degrades rapidly as channel conditions worsen, exhibiting a trend similar to that observed for the DeepJSCC scheme in previous experiments. The MDMA scheme benefits from high-fidelity analog transmission and

thus demonstrates excellent performance at high SL-SNR. However, as the channel quality deteriorates, its performance falls behind that of the CS-MDMA enhanced SFSC scheme.

We evaluate the computational complexity in terms of FLOPs, model parameters, and average inference time. The comparative results for processing $512 \times 512 \times 3$ images are detailed in Table III, while those for two-user downlink transmission are presented in Table IV. The experimental results indicate that, since SFSC adopts a more sophisticated network architecture to enhance reconstruction quality, its inference latency and computational complexity are higher than that of the lightweight DeepJSCC scheme. Nevertheless, compared with conventional digital semantic communication approaches such as RM-JCM, SFSC reduces the number of parameters by approximately 84%, reduces the number of FLOPs by approximately 78%, and achieves a significant improvement in runtime efficiency. It is observed that the proposed CS-MDMA incurs higher inference latency and computational complexity compared to the analog-based MDMA scheme. This increase is attributed to the more sophisticated neural network architecture employed to achieve superior spectral efficiency and image reconstruction performance. Since the NOMA and NOMA-JSCC schemes share a similar model structure, only the NOMA-JSCC scheme is listed for comparison. Notably, compared with NOMA-JSCC, CS-MDMA reduces the number of parameters by approximately 11.8% and reduces the FLOPs by about 24.7%. Consequently, the average runtime is reduced from 70.45 ms to 59.34 ms. These results demonstrate that the proposed scheme strikes a favorable trade-off between communication performance and computational overhead.

TABLE III: THE NUMBER OF FLOPs, THE NUMBER OF PARAMETERS AND RUNTIME OF COMPARED METHODS TESTED ON A $512 \times 512 \times 3$ IMAGE

Model	FLOPs (G)	Runtime (ms)	Params (M)
SFSC	61.442	45.60	2.895
TM-DeepJSCC	2.215	2.27	0.140
RM-DeepJSCC	4.430	3.67	0.140
TM-JCM	140.135	29.07	18.544
RM-JCM	280.270	60.23	18.544

TABLE IV: THE NUMBER OF FLOPs, THE NUMBER OF PARAMETERS AND RUNTIME FOR TWO USERS DOWNLINK TRANSMISSION

Model	FLOPs (G)	Runtime (ms)	Params (M)
CS-MDMA	255.432	59.34	2.267
MDMA	8.867	4.24	0.141
NOMA-JSCC	339.034	70.45	2.57

Although the proposed scheme entails a sophisticated network architecture compared to analog semantic communication schemes (e.g., DeepJSCC), the resulting complexity is well within the capabilities of satellite on-board processing hardware, which has evolved to support TFLOPs-level processing [58]. In terms of performance, the proposed scheme achieves significant improvements in image reconstruction

quality (measured by PSNR and MS-SSIM) and spectral efficiency, particularly in low SNR regimes. Moreover, compared to existing digital semantic communication schemes, our scheme not only enhances both image reconstruction quality and spectral efficiency but also reduces computational overhead. Furthermore, considering the scarce spectral resources in satellite networks, the proposed schemes effectively trades acceptable computational cost for significant bandwidth savings, which is a highly favorable trade-off for 6G satellite-terrestrial networks.

V. CONCLUSION

This paper has proposed an SFSC framework tailored for LEO satellite-terrestrial networks, addressing the critical challenges of severe path loss, time-varying channel conditions, and spectrum scarcity. By introducing a VQ-PEM, we achieve the joint optimization of semantic compression and constellation mapping, ensuring robust feature transmission. To mitigate the noise accumulation inherent in multi-hop relaying, we have developed the semantic forwarding mechanism. This mechanism allows satellite relays to perform lightweight semantic-level processing without the computational burden of full decoding and re-encoding. Furthermore, we have addressed the dynamic nature of satellite links through a channel-aware semantic reconstruction scheme, which leverages FiLM to adaptively fuse SNR information with semantic features. Finally, to enhance spectral efficiency in multi-user scenarios, we have extended the framework with a CS-MDMA method. Simulation results have demonstrated that the proposed SFSC scheme achieves a significant PSNR gain of approximately 7.9 dB in the low SNR regime compared to existing benchmarks. Moreover, the framework has reduced the number of model parameters by approximately 84% compared to conventional regenerative joint coding-modulation schemes, striking a favorable trade-off between semantic fidelity and on-board computational overhead. In the future, we will explore the integration of the CS-MDMA scheme and other advanced multiple access technologies, and extend the proposed SFSC framework to multi-hop scenarios in SAGIN.

REFERENCES

- [1] M. Z. Chowdhury, M. Shahjalal, S. Ahmed, and Y. M. Jang, "6g wireless communication systems: Applications, requirements, technologies, challenges, and research directions," *IEEE Open Journal of the Communications Society*, vol. 1, pp. 957–975, 2020.
- [2] D. C. Nguyen, M. Ding, P. N. Pathirana, A. Seneviratne, J. Li, D. Niyato, O. Dobre, and H. V. Poor, "6g internet of things: A comprehensive survey," *IEEE Internet of Things Journal*, vol. 9, no. 1, pp. 359–383, 2022.
- [3] M. Giordani and M. Zorzi, "Non-terrestrial networks in the 6g era: Challenges and opportunities," *IEEE Network*, vol. 35, no. 2, pp. 244–251, 2021.
- [4] Y. Xiao, Z. Ye, M. Wu, H. Li, M. Xiao, M.-S. Alouini, A. Al-Hourani, and S. Cioni, "Space-air-ground integrated wireless networks for 6g: Basics, key technologies, and future trends," *IEEE Journal on Selected Areas in Communications*, vol. 42, no. 12, pp. 3327–3354, 2024.
- [5] J. Liu, Y. Shi, Z. M. Fadlullah, and N. Kato, "Space-air-ground integrated network: A survey," *IEEE Communications Surveys & Tutorials*, vol. 20, no. 4, pp. 2714–2741, 2018.

- [6] M. M. Azari, S. Solanki, S. Chatzinotas, O. Kodheli, H. Sallouha, A. Colpaert, J. F. Mendoza Montoya, S. Pollin, A. Haqiqatnejad, A. Mostaani, E. Lagunas, and B. Ottersten, "Evolution of non-terrestrial networks from 5g to 6g: A survey," *IEEE Communications Surveys & Tutorials*, vol. 24, no. 4, pp. 2633–2672, 2022.
- [7] T. Pecorella, L. S. Ronga, F. Chiti, S. Jayousi, and L. Franck, "Emergency satellite communications: research and standardization activities," *IEEE Communications Magazine*, vol. 53, no. 5, pp. 170–177, 2015.
- [8] F. Babich, M. Comisso, A. Cuttin, M. Marchese, and F. Patrono, "Nanosatellite-5g integration in the millimeter wave domain: A full top-down approach," *IEEE Transactions on Mobile Computing*, vol. 19, no. 2, pp. 390–404, 2020.
- [9] J. Jiao, S. Liu, J. Ding, J. Huang, S. Wu, R. Lu, and Q. Zhang, "Age-optimal network coding harq transmission scheme for dual-hop satellite-integrated internet," *IEEE Transactions on Vehicular Technology*, vol. 71, no. 10, pp. 10666–10682, 2022.
- [10] J. Zhang, X. Li, I. S. Ansari, Y. Liu, and K. A. Qaraqe, "Performance analysis of dual-hop df satellite relaying over k - μ shadowed fading channels," in *2017 IEEE Wireless Communications and Networking Conference (WCNC)*, 2017, pp. 1–6.
- [11] "3rd generation partnership project; technical specification group radio access network; study on new radio (NR) to support non-terrestrial networks (release 15)," Tech. Rep. 3GPP TR 38.811 V15.4.0, Sep. 2020.
- [12] P. Yue, J. An, J. Zhang, J. Ye, G. Pan, S. Wang, P. Xiao, and L. Hanzo, "Low earth orbit satellite security and reliability: Issues, solutions, and the road ahead," *IEEE Communications Surveys & Tutorials*, vol. 25, no. 3, pp. 1604–1652, 2023.
- [13] Y. Su, Y. Liu, Y. Zhou, J. Yuan, H. Cao, and J. Shi, "Broadband leo satellite communications: Architectures and key technologies," *IEEE Wireless Communications*, vol. 26, no. 2, pp. 55–61, 2019.
- [14] O. Kodheli, E. Lagunas, N. Maturo, S. K. Sharma, B. Shankar, J. F. M. Montoya, J. C. M. Duncan, D. Spano, S. Chatzinotas, S. Kisseleff, J. Querol, L. Lei, T. X. Vu, and G. Goussetis, "Satellite communications in the new space era: A survey and future challenges," *IEEE Communications Surveys & Tutorials*, vol. 23, no. 1, pp. 70–109, 2021.
- [15] H. Xie, Z. Qin, G. Y. Li, and B.-H. Juang, "Deep learning enabled semantic communication systems," *IEEE Transactions on Signal Processing*, vol. 69, pp. 2663–2675, 2021.
- [16] W. Yang, H. Du, Z. Q. Liew, W. Y. B. Lim, Z. Xiong, D. Niyato, X. Chi, X. Shen, and C. Miao, "Semantic communications for future internet: Fundamentals, applications, and challenges," *IEEE Communications Surveys & Tutorials*, vol. 25, no. 1, pp. 213–250, 2023.
- [17] J. Huang, M. Sun, Y. Zhang, H. Wang, and X. Xu, "VQ-SDSC: Vector quantized satellite digital semantic communication framework," in *IEEE INFOCOM 2025 - IEEE Conference on Computer Communications Workshops (INFOCOM WKSHPS)*, 2025, pp. 1–2.
- [18] X. Luo, H.-H. Chen, and Q. Guo, "Semantic communications: Overview, open issues, and future research directions," *IEEE Wireless Communications*, vol. 29, no. 1, pp. 210–219, 2022.
- [19] H. Xie, Z. Qin, X. Tao, and K. B. Letaief, "Task-oriented multi-user semantic communications," *IEEE Journal on Selected Areas in Communications*, vol. 40, no. 9, pp. 2584–2597, 2022.
- [20] E. Bourtsoulatzé, D. Burth Kurka, and D. Gündüz, "Deep joint source-channel coding for wireless image transmission," *IEEE Transactions on Cognitive Communications and Networking*, vol. 5, no. 3, pp. 567–579, 2019.
- [21] J. Dai, S. Wang, K. Tan, Z. Si, X. Qin, K. Niu, and P. Zhang, "Nonlinear transform source-channel coding for semantic communications," *IEEE Journal on Selected Areas in Communications*, vol. 40, no. 8, pp. 2300–2316, 2022.
- [22] E. Erdemir, T.-Y. Tung, P. L. Dragotti, and D. Gündüz, "Generative joint source-channel coding for semantic image transmission," *IEEE Journal on Selected Areas in Communications*, vol. 41, no. 8, pp. 2645–2657, 2023.
- [23] P. Zhang, X. Xu, C. Dong, K. Niu, H. Liang, Z. Liang, X. Qin, M. Sun, H. Chen, N. Ma *et al.*, "Model division multiple access for semantic communications," *Frontiers of Information Technology & Electronic Engineering*, vol. 24, no. 6, pp. 801–812, 2023.
- [24] I. Ahmed, Y. Sun, J. Fu, A. Köse, L. Musavian, M. Xiao, and B. Özbek, "Semantic communications in 6g: Coexistence, multiple access, and satellite networks," *IEEE Communications Standards Magazine*, vol. 9, no. 4, pp. 58–64, 2025.
- [25] Y. Zhang, B. Xu, S. Han, and X. Xu, "Multi-task driven semantic communication for satellite imagery," in *ICC 2025 - IEEE International Conference on Communications*, 2025, pp. 2460–2465.
- [26] T.-Y. Tung, D. B. Kurka, M. Jankowski, and D. Gündüz, "Deepjsecq: Constellation constrained deep joint source-channel coding," *IEEE Journal on Selected Areas in Information Theory*, vol. 3, no. 4, pp. 720–731, 2022.
- [27] Q. Fu, H. Xie, Z. Qin, G. Slabaugh, and X. Tao, "Vector quantized semantic communication system," *IEEE Wireless Communications Letters*, vol. 12, no. 6, pp. 982–986, 2023.
- [28] Y. Bo, Y. Duan, S. Shao, and M. Tao, "Joint coding-modulation for digital semantic communications via variational autoencoder," *IEEE Transactions on Communications*, vol. 72, no. 9, pp. 5626–5640, 2024.
- [29] W. Chen, S. Li, C. Ju, D. Wang, J. Li, and D. Wang, "Semantic-enhanced downlink leo satellite communication system with ofds modulation," *IEEE Communications Letters*, vol. 28, no. 6, pp. 1377–1381, 2024.
- [30] Z. Lin, H. Lin, Y. Sun, S. Basheer, M. Tabrez Quasim, and K. Dev, "Joint coding and modulation for robust semantic communication in satellite communications," *IEEE Internet of Things Journal*, vol. 13, no. 1, pp. 339–346, 2026.
- [31] V.-P. Bui, T. Q. Dinh, I. Leyva-Mayorga, S. R. Pandey, E. Lagunas, and P. Popovski, "Semantic image encoding and communication for earth observation with leo satellites," *IEEE Transactions on Cognitive Communications and Networking*, vol. 11, no. 2, pp. 1210–1224, 2025.
- [32] P. Jiang, C.-K. Wen, X. Li, S. Jin, and G. Y. Li, "Semantic satellite communications based on generative foundation model," *IEEE Journal on Selected Areas in Communications*, vol. 43, no. 7, pp. 2431–2445, 2025.
- [33] S. Ma, W. Liang, B. Zhang, and D. Wang, "An investigation on intelligent relay assisted semantic communication networks," in *2023 IEEE Wireless Communications and Networking Conference (WCNC)*, 2023, pp. 1–6.
- [34] X. Luo, B. Yin, Z. Chen, B. Xia, and J. Wang, "Autoencoder-based semantic communication systems with relay channels," in *2022 IEEE International Conference on Communications Workshops (ICC Workshops)*, 2022, pp. 711–716.
- [35] W. An, Z. Bao, H. Liang, C. Dong, and X. Xu, "A relay system for semantic image transmission based on shared feature extraction and hyperprior entropy compression," *IEEE Internet of Things Journal*, vol. 11, no. 9, pp. 16158–16170, 2024.
- [36] Z. Lin, M. Lin, T. de Cola, J.-B. Wang, W.-P. Zhu, and J. Cheng, "Supporting iot with rate-splitting multiple access in satellite and aerial-integrated networks," *IEEE Internet of Things Journal*, vol. 8, no. 14, pp. 11123–11134, 2021.
- [37] Y. Zhang, H. Zhang, H. Zhou, K. Long, and G. K. Karagiannidis, "Resource allocation in terrestrial-satellite-based next generation multiple access networks with interference cooperation," *IEEE Journal on Selected Areas in Communications*, vol. 40, no. 4, pp. 1210–1221, 2022.
- [38] H. Liang, K. Liu, X. Liu, H. Jiang, C. Dong, X. Xu, K. Niu, and P. Zhang, "Orthogonal model division multiple access," *IEEE Transactions on Wireless Communications*, vol. 23, no. 9, pp. 11693–11707, 2024.
- [39] D. Wu, Z. Zhang, Y. Meng, X. Qin, and Y. Liu, "Joint deep adversarial semantic decomposition scheme for model division multiple access in iot," in *2025 IEEE Wireless Communications and Networking Conference (WCNC)*, 2025, pp. 01–06.
- [40] S. Ma, Z. Sun, B. Shen, Y. Wu, H. Li, G. Shi, S. Li, and N. Al-Dhahir, "Semantic feature division multiple access for digital semantic broadcast channels," *IEEE Internet of Things Journal*, vol. 12, no. 11, pp. 17123–17136, 2025.
- [41] L. You, K.-X. Li, J. Wang, X. Gao, X.-G. Xia, and B. Ottersten, "Massive mimo transmission for leo satellite communications," *IEEE Journal on Selected Areas in Communications*, vol. 38, no. 8, pp. 1851–1865, 2020.
- [42] L. You, X. Gao, A. L. Swindlehurst, and W. Zhong, "Channel acquisition for massive mimo-ofdm with adjustable phase shift pilots," *IEEE Transactions on Signal Processing*, vol. 64, no. 6, pp. 1461–1476, 2016.
- [43] N. Letzepis and A. J. Grant, "Capacity of the multiple spot beam satellite channel with rician fading," *IEEE Transactions on Information Theory*, vol. 54, no. 11, pp. 5210–5222, 2008.
- [44] A. van den Oord, O. Vinyals, and k. kavukcuoglu, "Neural discrete representation learning," in *Advances in Neural Information Processing Systems*, vol. 30, 2017.
- [45] L. Liu, C. Dong, X. Liu, B. Yu, and J. Gao, "Bridging discrete and backpropagation: Straight-through and beyond," in *Advances in Neural Information Processing Systems*, vol. 36, 2023, pp. 12291–12311.
- [46] Y. Bengio, N. Léonard, and A. Courville, "Estimating or propagating gradients through stochastic neurons for conditional computation," *arXiv preprint arXiv:1308.3432*, 2013.
- [47] E. Jang, S. Gu, and B. Poole, "Categorical reparameterization with gumbel-softmax," *arXiv preprint arXiv:1611.01144*, 2016.

- [48] E. Perez, F. Strub, H. De Vries, V. Dumoulin, and A. Courville, "Film: Visual reasoning with a general conditioning layer," in *Proceedings of the AAAI conference on artificial intelligence*, vol. 32, no. 1, 2018.
- [49] R. Liu, J. Lehman, P. Molino, F. Petroski Such, E. Frank, A. Sergeev, and J. Yosinski, "An intriguing failing of convolutional neural networks and the coordconv solution," in *Advances in Neural Information Processing Systems*, vol. 31, 2018.
- [50] R. Linsker, "Towards an organizing principle for a layered perceptual network," in *Neural Information Processing Systems*, vol. 0, 1987.
- [51] D. Barber and F. Agakov, "Information maximization in noisy channels : A variational approach," in *Advances in Neural Information Processing Systems*, vol. 16, 2003.
- [52] S. S. Schoenholz, J. Gilmer, S. Ganguli, and J. Sohl-Dickstein, "Deep information propagation," in *International Conference on Learning Representations (ICLR)*, 2017.
- [53] X. Glorot and Y. Bengio, "Understanding the difficulty of training deep feedforward neural networks," in *Proceedings of the Thirteenth International Conference on Artificial Intelligence and Statistics*, vol. 9, May 2010, pp. 249–256.
- [54] D. P. Kingma and M. Welling, "Auto-encoding variational bayes," in *International Conference on Learning Representations (ICLR)*, April 2014.
- [55] Z. Wang, A. Bovik, H. Sheikh, and E. Simoncelli, "Image quality assessment: from error visibility to structural similarity," *IEEE Transactions on Image Processing*, vol. 13, no. 4, pp. 600–612, 2004.
- [56] Z. Wang, E. Simoncelli, and A. Bovik, "Multiscale structural similarity for image quality assessment," in *The Thirty-Seventh Asilomar Conference on Signals, Systems & Computers, 2003*, vol. 2, 2003, pp. 1398–1402 Vol.2.
- [57] M. Cordts, M. Omran, S. Ramos, T. Rehfeld, M. Enzweiler, R. Benenson, U. Franke, S. Roth, and B. Schiele, "The cityscapes dataset for semantic urban scene understanding," in *Proceedings of the IEEE Conference on Computer Vision and Pattern Recognition (CVPR)*, June 2016.
- [58] B. Denby and B. Lucia, "Orbital edge computing: Machine inference in space," *IEEE Computer Architecture Letters*, vol. 18, no. 1, pp. 59–62, 2019.